Global and Planetary Change 204 (2021) 103547

Contents lists available at ScienceDirect

Global and Planetary Change

journal homepage: www.elsevier.com/locate/gloplacha

The 'pargasosphere' hypothesis: Looking at global plate tectonics from a new perspective

István J. Kovács [a,b,c,*], Nóra Liptai [a,b,c], Alexander Koptev [d], Sierd A.P.L. Cloetingh [b,e], Thomas P. Lange [a,f,g], Liviu Matenco [e], Alexandru Szakács [h], Mircea Radulian [i,j], Márta Berkesi [a,f], Levente Patkó [a,b,f], Gábor Molnár [b,k,l], Attila Novák [a,b], Viktor Wesztergom [b], Csaba Szabó [b,f], Tamás Fancsik [m]

[a] MTA EK Lendület Pannon LitH$_2$Oscope Research Group, Centre for Energy Research, Budapest, Hungary
[b] Institute of Earth Physics and Space Science (ELKH EPSS), Sopron, Hungary
[c] Centre for Energy Research, Institute for Energy Security and Environmental Safety, Budapest, Hungary
[d] University of Tübingen, Department of Geosciences, Tübingen, Germany
[e] Tectonics Group, Department of Earth Sciences, Faculty of Geosciences, Utrecht University, Utrecht, Netherlands
[f] Lithosphere Fluid Research Lab (LRG), Eötvös Loránd University, Budapest, Hungary
[g] Isotope Climatology and Department of Environmental Research Centre, Institute for Nuclear Research (ATOMKI), Debrecen, Hungary
[h] Institute of Geodynamics, Romanian Academy, Bucharest, Romania
[i] National Institute of Earth Physics, Bucharest, Romania
[j] Academy of Romanian Scientists, Bucharest, Romania
[k] Geological, Geophysical and Space Research Group of the Hungarian Academy of Sciences at Eötvös Loránd University, Budapest, Hungary
[l] Óbuda University, Alba Regia Technical Faculty, Institute of Geoinformatics, Székesfehérvár, Hungary
[m] Mining and Geological Survey of Hungary, Budapest, Hungary

ARTICLE INFO

Editor: Zhengtang Guo

Keywords:
Water
Pargasite
Plate tectonics
Lithosphere
Asthenosphere
Mid-lithospheric discontinuities

ABSTRACT

Apart from the lithosphere-asthenosphere boundary (LAB), mid-lithospheric discontinuities (MLDs) in thick and old continental lithospheres appear to play an important role in global plate tectonics. Initiation of intra-continental subduction, delamination of the lower continental lithospheric mantle and removal of cratonic roots are likely to occur along MLDs.

Here we introduce the 'pargasosphere' hypothesis which could account for the origin of both boundaries. The observation that pargasitic amphibole is stable even at very low bulk 'water' concentration (~a few hundreds ppm wt.) implies that the solidus of the shallow upper mantle (<3 GPa) is usually the pargasite dehydration solidus at ~1100 °C. In young continental and oceanic lithosphere (<70 Ma) this solidus defines the LAB. The LAB separates the deeper, partial melt bearing asthenosphere from the shallower melt barren lithosphere, explaining their contrasting rheology.

In old continents pargasite breaks down at the sub-solidus pargasite dehydration boundary at ~3 GPa and liberates 'water'-rich fluids. This latter process may be responsible for the formation of MLDs. The occurrence of partial melts or fluids beyond the pargasite stability field can explain commonly observed geophysical anomalies associated with the LAB and MLDs.

We present forward modelled variations of shear wave velocity and resistivity at the LAB and MLDs for idealised lithospheric columns. These columns are constructed based on the 'pargasosphere' hypothesis and geotherms corresponding to continental lithospheres with various tectono-thermal ages. The 'pargasosphere' hypothesis offers a number of other empirically testable implications. For instance, cooling asthenosphere beneath young extensional continental and oceanic lithosphere settings can be the source of surface CO_2 emanations even at locations distant from areas with active volcanoes. The Vrancea zone (Eastern Europe) appears to be a suitable site for testing the 'pargasosphere' hypothesis for elucidating the origin of intermediate-depth earthquakes (70–300 km) and to explain the delamination of the lower continental lithospheric mantle.

* Corresponding author.
E-mail address: kovacs.istvan.janos@csfk.mta.hu (I.J. Kovács).

https://doi.org/10.1016/j.gloplacha.2021.103547
Received 1 July 2020; Received in revised form 22 May 2021; Accepted 14 June 2021
Available online 18 June 2021

1. Introduction

'Water' is a vital element for life, but also an indispensable 'ingredient' for maintaining Earth as a geologically living planet (e.g., Peslier et al., 2017; Rychert et al., 2020). Plate tectonics postulates that the Earth's rigid outer shell, the lithosphere, 'floats' on the underlying less viscous asthenosphere (e.g., Anderson, 1975; Davies, 1992). The reasons for their contrasting rheological behaviour (cf. Green, 1973, 2015; Karato, 2012) are still unclear and controversial even many decades after the birth of the modern plate tectonic theory (Raff and Mason, 1961; Dietz, 1962). The asthenosphere is commonly characterised by slower propagation and higher attenuation of seismic waves, higher electrical conductivity, higher degree of anisotropy, higher strain rate and lower viscosity than the overlying lithosphere (e.g., Eaton et al., 2009; Fischer et al., 2010). The variation of these properties occurs in a relatively narrow depth interval typically from a few kilometres to ~30 km in extreme cases (Rychert et al., 2020). Several models attributed these variations of the geophysical properties to solid-state processes including grain size variations (Austin and Evans, 2007), changing redox conditions (Cline Ii et al., 2018), elastically accommodated grain boundary sliding (Karato, 2012; Karato, 2014; Karato et al., 2015) or changing anisotropy (Rychert et al., 2007, 2012). These explanations have been able to explain some of the observed features of the lithosphere-asthenosphere interface but failed to explain others. The presence of small amounts of partial melt in the asthenosphere has been also proposed to explain the origin of the lithosphere-asthenosphere boundary (referred to as LAB; Debayle et al., 2020; Rychert et al., 2020). However, convincing geochemical explanations, regarding why melting happens in the ambient upper mantle at pressure, temperature and oxygen fugacity conditions characteristic for the LAB have been lacking. Another challenge concerns the definition of the bottom of the lithosphere (i.e., LAB), which can vary depending on its link to different physical properties (Fig. 1; e.g., Artemieva, 2009; Eaton et al., 2009).

Due to the improvement of geophysical techniques and large-scale national and international projects in the past few decades further tectonically important boundaries have been discovered in the thick (>100 km) and old continental lithospheric mantle (Thybo, 2006; Rader et al., 2015; Selway et al., 2015; Hopper and Fischer, 2015; Saha et al., 2021). The so-called mid-lithospheric discontinuities (MLDs) are characterised by a significant reduction (2–6%) in shear wave velocities in a relatively narrow depth interval (of a few kilometres) usually between 80–100 km depths (e.g., Hopper and Fischer, 2015; Selway et al., 2015; Saha et al., 2021). Akin to the LAB numerous and sometimes similar explanations have been developed for the sharp drop in shear wave velocity at MLDs depths including change in anisotropy, elastically accommodated grain boundary sliding, and the presence of hydrous minerals and partial melts (Selway et al., 2015; Rader et al., 2015; Aulbach et al., 2017; Saha and Dasgupta, 2019; Saha et al., 2021). So far none of the proposed models can fully account for the observations at these prominent discontinuities. Thus, it seems that a comprehensive understanding of the role and nature of the LAB and MLDs remains an ultimate challenge for solid Earth sciences. In our paper we revisit and develop further a so far overlooked hypothesis that the (melting) properties of hydrous mineral bearing ambient upper mantle can explain the origin of MLDs in old continental lithospheres and the LAB in younger ones. We also show how the seemingly contrasting definitions of the base of the lithosphere (i.e., LAB) can be reconciled with each other, bridging the gap between geophysical and geochemical approaches. Examples are given of how and where the predictions of this hypothesis can be tested.

The 'pargasosphere' hypothesis offers an alternative explanation and model for how the cooling asthenosphere below young and thin (<100 km) oceanic and continental lithospheres distant to active volcanism can be the source of diffuse CO_2 emanations on the surface. CO_2 may be enriched and accumulated from crystallising incipient partial melts as CO_2 is concentrated in residual fluids in inclusions or along grain boundaries. These CO_2-rich fluids can then migrate towards the surface due to their high mobility, buoyancy and favourable stress field in the upper mantle.

Initial geochemical and petrophysical forward models are constructed based on realistic upper mantle compositions and different geotherms to predict the variation of resistivity and shear wave velocity across the LAB and MLD. The predicted changes in physical properties hold also the potential to improve geodynamic models in the future.

In this paper, a geodynamic outlook is given on how predicted weakness zones along the MLD can contribute to the delamination of the

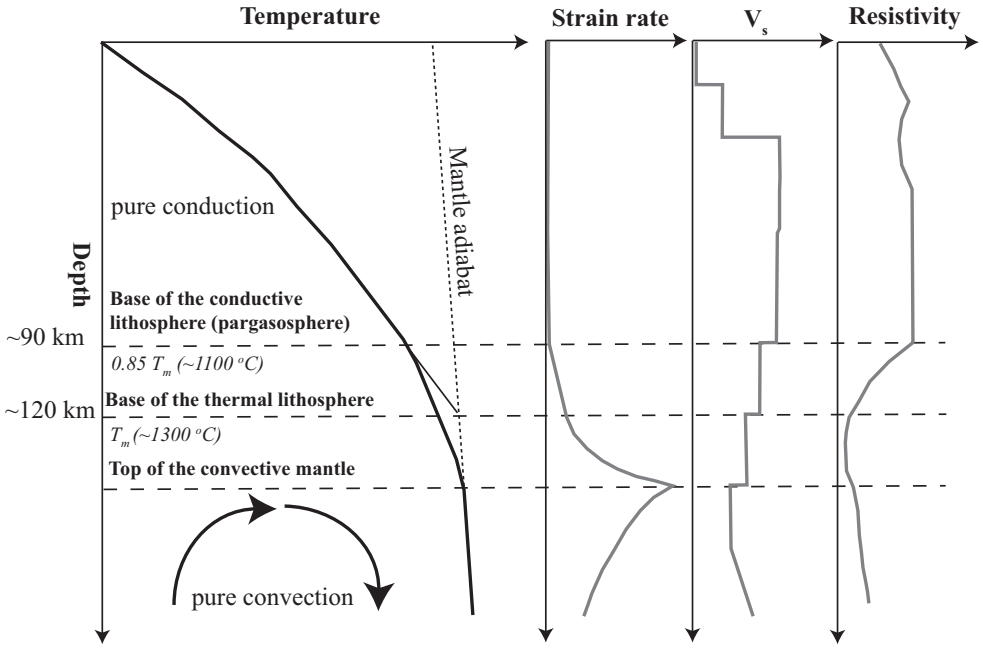

Fig. 1. The base of the lithosphere (i.e., lithosphere-asthenosphere boundary: LAB) is usually defined according to the temperature dependent variation in physical properties. The LAB can be defined as the base of the conductive lithosphere, the bottom of the thermal lithosphere or top of the convective mantle among many other equally valid definitions. The base of the thermal lithosphere is at the intersection of the linear extension of the conductive geotherm and the mantle adiabat. The figure is modified after Fig. 1 in Artemieva (2009). The schematic geotherm corresponds to ~60 mW/m^2 surface heat flow which is close to the average continental heat flow (Pollack and Chapman, 1977). The variations of strain rate, shear wave velocity and resistivity are also displayed as a function of temperature (modified after Fig. 2 in Eaton et al., 2009). Note that sudden changes in all these physical properties begin at the base of the conductive lithosphere but reach their extreme values deeper, close the base of the thermal lithosphere. This latter boundary may also coincide with a chemical boundary separating melt bearing and barren parts of the upper mantle along the pargasite dehydration solidus (see text for further discussion).

lower part of the lithospheric mantle The Vrancea seismogenic zone appears to be an excellent target for the study of delamination of the lower continental lithosphere and its possible role in generating intermediate-depth earthquakes.

2. Definitions of the LAB and MLD and development of the 'pargasosphere' hypothesis

2.1. Controversial LAB definitions

The LAB is commonly defined by a temperature-dependent drop in mantle viscosity when it becomes sufficiently low to allow the deformation necessary to accommodate the movement of lithospheric plates with respect to the underlying weak mantle (i.e., the asthenosphere). Traditionally, this transition from 'high' to 'low' viscosity is defined for fully 'dry' mantle (i.e., without any fluids and partial melting), and corresponds to the 1300 °C isotherm (thermal' lithosphere, e.g., Artemieva and Mooney, 2001; Artemieva, 2006; Eaton et al., 2009; Koptev and Ershov, 2010, 2011). Olivine is the major mineral constituent of the upper mantle (>50 v/v%), and consequently its deformation properties determine the viscosity of the upper mantle. At temperatures >1000 °C olivine deforms by high temperature dislocation and diffusion creep (Mei et al., 2010). However, the associated degree and depth of the predicted viscosity drop appear to be incompatible with those typically observed for the LAB (Behn et al., 2009; Rychert et al., 2020). Note that there are also results which assume somewhat higher overall viscosity for the asthenosphere and less significant viscosity contrast between the lithosphere and asthenosphere (e.g., Fjeldskaar, 1994). The geodynamic models usually assume gradual P-T and stress-dependent decrease of strength (or effective viscosity) within the ductile part of the lithospheric mantle and underlying asthenosphere (e.g., Duretz and Gerya, 2013; Li et al., 2016). Thus, other factors are needed to explain the viscosity reduction at the LAB that may not be explained by sub-solidus processes alone. Nevertheless, the ~1300 °C isotherm is commonly regarded as the base of the thermal lithosphere, where the viscosity of the upper mantle gradually becomes low enough to enable convection (e.g., McKenzie, 1967; Pollack and Chapman, 1977; Eaton et al., 2009; Garel and Thoraval, 2021). The depth of this 1300 °C isotherm is located between the base of the conductive lithosphere and the top of the convective upper mantle (Fig. 1). For a surface heat flow typical for mature continental lithospheres adopted (~60 mW/m^2, Artemieva, 2009; Davies and Davies, 2010; Davies, 2013), the 1300 °C isotherm is at ~120 km depth. This is also the depth where the conductive geotherm would intersect the mantle adiabat (Fig. 1). The 120 km depth and 1300 °C temperature also correspond to the initial thickness of the thermal lithosphere in stretching models for matur continental lithospheres in thermal equilibrium (McKenzie, 1978; Royden and Keen, 1980).

Pollack and Chapman (1977) demonstrated that the temperature of the actual (i.e., constrained by seismology and magnetotellurics) LAB agrees well with 85% of the 'absolute solidus temperature' (T_m). In their paper this 'LAB' temperature was empirically calibrated using the observed relationship between global surface heat flow values and detected LAB depths. The authors proposed that if the average continental heatflow is ~60 mW/m^2 the temperature of the LAB is ~1100 °C at ~90 km depth (Fig. 1). Nevertheless, they did not discuss further the reasons why the LAB should coincide with the 0.85 T_m.

Note that these definitions concerning the base of the lithosphere considered only sub solidus processes and disregarded the effect of volatiles on physical properties of upper mantle minerals. It has not been explained why the LAB determinations on average fit better the base of the conductive lithosphere which is shallower (by ~30 km) and cooler (by ~200 °C) than the base of the thermal lithosphere. It should also be mentioned that at the time, experimental and analytical methodologies and facilities were not available to fully explore the role of small amounts of volatiles play in determining the melting temperature of the ambient upper mantle. In the following we present a hypothesis which has the capacity to integrate these seemingly contrasting definitions of the LAB into a new coherent framework. In addition, it can also bridge the gap between geophysical and geochemical observations if the effect of a trace amount of 'water' is considered.

2.2. The role of trace amounts of 'water' and hydrous phases in the shallow upper mantle

The hypothesis presented in this paper involves the 'hydrous' Earth where the important role of 'trace' amounts of volatiles is taken into account. The rapid development of analytical techniques and methodologies has made it possible to analyse the volatile contents of upper mantle rocks and experimental samples with unprecedented sensitivity and spatial resolution. Among many techniques Secondary Ion-Mass Spectrometry (SIMS) and micro-Fourier Transform Infrared spectrometry (micro-FTIR) have become the most popular and widely applied ones (e.g., Rossman, 2006). Although SIMS has excellent spatial resolution (few tens of μm) and sensitivity (at the ppm wt. levels), it only detects bulk concentrations (Hauri et al., 2002). Thus, SIMS is unable to identify the incorporation mechanism of the analysed species (i.e., whether it originates from fluid inclusions, minerals or grain boundaries). Micro-FTIR has similar sensitivity and is able to identify the incorporation mechanism but its spatial resolution is weaker (>50 μm; e.g., Libowitzky and Rossman, 1996; Beran and Libowitzky, 2006; Kovács et al., 2008). No wonder that although it has been known since the ~60's (e.g., Kats, 1961) that volatiles, 'water' in particular, can be incorporated into vacancies of minerals in trace amounts, it is only in the past two decades that our knowledge on the concentration and distribution of volatiles in the upper mantle has advanced rapidly (e.g., Ingrin and Skogby, 2000; Peslier, 2010; Demouchy and Bolfan-Casanova, 2016; Peslier et al., 2017; Xia et al., 2019; Liptai et al., 2021).

The dominant mineral constituents of the upper mantle are the nominally anhydrous minerals (referred to as NAMs hereafter, i.e., olivine, pyroxenes and garnet). The NAMs do not contain 'water' in their mineral formulae and incorporate only trace amounts of 'water' as structural hydroxyl in sporadic vacancies of their crystal lattice (up to ~1000 ppm wt. or 0.1 wt.%; Beran, 1976; Kohlstedt et al., 1996; Mosenfelder et al., 2006; Kovács et al., 2010, 2012; Peslier et al., 2010; Demouchy and Bolfan-Casanova, 2016; Xia et al., 2019). In the vacancies the structural hydroxyl consists of a proton (H^+) attached to one of the coordinating oxygens and charge balances alone or in coupled substitutions for the missing central cation (e.g., Stalder and Ludwig, 2007; Kovács et al., 2010; Blanchard et al., 2017). The structural hydroxyl content in NAMs is expressed in molecular water equivalent in ppm wt. (equals to 0.0001 wt.% and referred to as ppm hereafter) and we will generally refer to this as the 'water' content of NAMs.

It has been revealed over the past decades that olivine, orthopyroxene and clinopyroxne contain up to ~100, ~350 and ~700 ppm 'water', respectively, in upper mantle xenoliths worldwide (Peslier, 2010; Demouchy and Bolfan-Casanova, 2016). Consequently the maximum bulk water content of the NAMs in the upper mantle is ~ 200 ppm if the presence of hydrous phases is disregarded. These maximum values typical for NAMs in natural upper mantle xenoliths are in excellent agreement with experimental studies which found similar 'water' concentrations even at very low bulk 'water' contents (~few hundred ppm wt.%; Green et al., 2010; 2014; Kovács et al., 2012). Estimates for the bulk 'water' content of the deeper asthenosphere provide higher values from 200 to 6000 ppm, based on clinopyroxene phenocrysts in basaltic magmas (Xia et al., 2019; Kovács et al., 2020). There is a variation in the average 'water' content of the asthenosphere for different tectonic environments since it is 50-250 ppm at mid-ocean ridges (MOR) (Saal et al., 2002) but higher (300-1000 ppm) below ocean islands (OI) and enriched MORs (Dixon et al., 2002).

This trace amount of 'water' has a disproportionately large effect on the physical properties of NAMs. 'Water' is known to increase

conductivity (e.g., Jones et al., 2012; Fullea, 2017), enhance seismic attenuation (Artemieva et al., 2004; Aizawa et al., 2008), affect the dominant deformation mechanism (Mackwell and Paterson, 1985; Demouchy et al., 2012; Girard et al., 2013) and reduce effective viscosity (Dixon et al., 2004; Li et al., 2008). The important effect of 'water' on minerals' structure is the so called hydrolytic weakening mechanism. This mechanism implies that the presence of protons (i.e., H^+), as structural hydroxyls in vacancies of NAMs, might favour dislocation climb which facilitates dislocation glide (Griggs, 1967; Kohlstedt, 2006; Girard et al., 2013; Tielke et al., 2017). This causes weakening of the crystal structure and is thought to increase with increasing 'water' content. This effect is operational even at very low 'water' contents when no free fluid or melt phases are present.

Compared to NAMs, hydrous minerals in the upper mantle incorporate even more 'water', as per their mineral formulae. The most common hydrous minerals are amphibole and phlogopite. Amphibole is a double-chain silicate mineral, which contains up to 2 wt.% 'water' as hydroxyls regularly incorporated in its crystal lattice (unlike structural hydroxyl incorporated in a much smaller amount in isolated point defects of NAMs). Amphibole is a mineral solid solution, in which numerous cation and anion substitutions are possible in different crystallographic sites, but anions may play only a subordinate role in the upper mantle. Thus, the chemical composition of amphibole can vary over a wide range of physico-chemical conditions. The most common amphibole in the upper mantle is pargasite (e.g., Niida and Green, 1999; Szabó et al., 2004; Kovács et al., 2012; Denis et al., 2015; Demouchy and Bolfan-Casanova, 2016). Its idealised mineral formula is $NaCa_2(Mg_4Al)(Si_6Al_2)O_{22}(OH)_2$ (Leake et al., 1997; Hawthorne et al., 2012). There are, however, other amphiboles in the upper mantle of K-richterite, hornblende, Mg-hastingsite and kearsutite compositions in subordinate modal abundance (Foley, 1991; Konzett, 1997; Konzett and Ulmer, 1999; Szabó et al., 2004). Pargasitic amphibole is stable at pressures and temperatures less than ~3 GPa and ~1100 °C respectively but can slightly vary with chemistry (Niida and Green, 1999; Mandler and Grove, 2016). K-richterite has a wider stability field and it is stable up to ~1450 °C at 9–10 GPa (Konzett and Ulmer, 1999; Trønnes, 2002). The modal abundance of amphibole in the ambient shallow peridotitic upper mantle can be as high as 20 v/v%, but it remains typically below 10 v/v % (Demouchy and Bolfan-Casanova, 2016). The latter authors found that the 'water' content of olivine (the most abundant NAMs in the upper mantle) slightly decreases with the increasing modal abundance of amphibole. The olivine 'water' content is typically in the 20–50 ppm range if there is less than 5 v/v% amphibole but below 20 ppm when amphibole exceeds 5 v/v%.

Phlogopite, a hydrous layer silicate, is also a well-known constituent of the shallow upper mantle containing ~10 wt.% 'water' and K_2O. It is stable at 4–5 GPa up to 1350 °C (Trønnes, 2002) and its modal abundance is typically only a few v/v% (e.g., Selway et al., 2015; Saha et al., 2021).

In addition to solid phases, 'water' can be incorporated in fluids and melts in higher concentrations reaching up to 30 wt.% (Green, 2015) in small amount of incipient hydrous silicate melts at lithospheric pressures.

2.3. The 'hydrous' solidus of the upper mantle and its relation to the MLD and LAB

The solidus is the temperature at which melting begins at a given pressure. Early experimental studies discovered the importance of pargasitic amphibole in influencing the solidus temperature (e.g., Green, 1973; Green and Liebermann, 1976). Due to the analytical and methodological developments in the past decades it has been demonstrated only recently that these solidus determinations are also accurate at trace bulk 'water' contents (few hundreds ppm; Asimow et al., 2004; Green et al., 2010; 2014; Kovács et al., 2012; Green, 2015). These experiments included the two most important volatile species in the upper mantle: H_2O and CO_2. Other experimental and theoretical studies on the solidus of the upper mantle have either not considered the role of pargasite at all (e.g., Katz et al., 2003; Grove et al., 2006; Hirschmann, 2010) or even if considered, its significance was assumed to be relevant only at higher bulk 'water' contents (Dasgupta, 2018; Saha et al., 2021).

In summary, studies which addressed the role of trace amounts of water and pargasite, concluded that the solidus of the upper mantle is the 'pargasite dehydration solidus' at pressures less than ~3 GPa and bulk 'water' contents between ~200 ppm and 0.4 wt.% (which is common in the shallow upper mantle too, Fig. 2, Fig. 12 in Green, 2015). In this case, the pargasite dehydration solidus temperature is ~1100 °C and basically does not depend on pressure, apart from a small interval before it joins the 'water saturated' solidus at ~ 3 GPa where it shows a negative Clapeyron-slope (i.e., $\Delta T/\Delta P<0$, Fig. 2a). Considering the properties of the average upper mantle, the pargasite dehydration solidus appears to best represent melting relations at pressures less than 3 GPa. At higher pressures, the solidus is the water saturated solidus if the bulk water content exceeds 200 ppm, which is generally the case in the ambient upper mantle. The important tectonic significance of these solidus curves becomes obvious when interpreted in the light of geotherms typical for lithospheres with different ages as follows.

1) Under higher surface heat flow (>~65 mW/m^2), a hot geotherm reaches 1100 °C (pargasite dehydration solidus) when the pressure is less than 3 GPa (shallower than ~100 km depth). In this case, the LAB is defined by the transition from sub-solidus state to an incipient partial melting regime with less than 1 v/v% melt. Melting always happens at ~1100 °C regardless of the pressure (Fig. 2a). This thermal regime is typical for Late Paleozoic and younger continental plates and young oceanic lithospheres (<70 Ma; Pollack and Chapman, 1977; Artemieva, 2009). In this case the pargasite dehydration solidus defines the LAB, which separates the melt-bearing asthenosphere from the solid lithosphere. The depth of the LAB can vary from ~ 0 km at mid-oceanic ridges to ~90 km in continental and old oceanic lithospheres.
2) Under intermediate surface heat flow values (50–65 mW/m^2), the geotherm reaches the pargasite dehydration solidus (1100 °C) at ~90-100 km and is still above the water saturated solidus below this depth (Fig. 2b). This thermal regime is typical for Early Paleozoic and Late Proterozoic continental plates and old oceanic plates (>70 Ma), but this regime also includes some relatively young cratons. In this case the depth of the LAB is ~90 km or deeper separating the silicate melt bearing asthenosphere from the solid lithosphere. For young cratons, the upper mantle may be depleted and dry enough that the bulk 'water' content remains below 200 ppm. This means that the geotherm may not necessarily intersect the water saturated solidus implying a deeper LAB. This intermediate thermal regime includes the kink in the pargasite dehydration solidus which can account for the formation of MLDs in young cratonic lithospheres, as discussed in detail further on.

This is the point where the contrasting definitions of the LAB can be reconciled. When the heat flow is ~60 mW/m^2, the pargasite dehydration solidus occurs at ~90–100 km depth and ~1100 °C, separating the solid lithosphere from the deeper incipient melt bearing (< 1v/v%) asthenosphere. The presence of a small amount of partial melt explains the decreasing seismic velocity (Chantel et al., 2016), electrical resistivity (Sifré et al., 2014) and increasing strain rate (Fig. 1; Kohlstedt and Zimmerman, 1996). This boundary coincides, therefore, with the base of the conductive lithosphere, which is also a geochemical boundary. The numerical parameterisation of olivine flow laws also indicated a good agreement between the depth of LAB indications in oceanic lithosphere and calculated viscosities, both close to the depth of the 1100 °C isotherm in half space cooling models (Behn et al., 2009; Rychert et al., 2020). Likewise, Niu and Green (2018) and Kovács et al. (2017) found that the 1100 °C isotherm falls very closely to the depth of

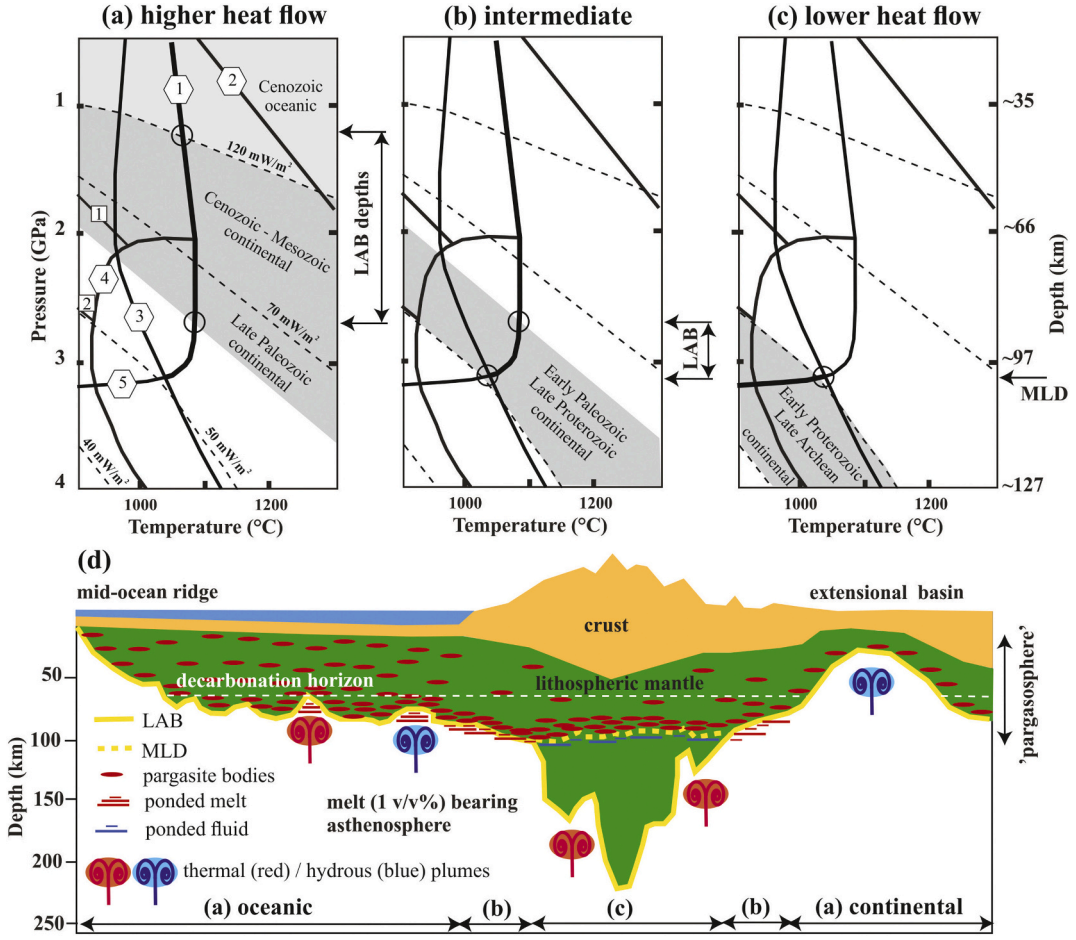

Fig. 2. Relationship between various solidi and geotherms typical for different tectono-thermal ages of the (continental) lithosphere. Three different scenarios are considered corresponding to a) young continental and oceanic lithospheres represented by higher heat flow (>~65 mW/m^2); b) old continental and oceanic lithospheres, and youngest cratons characterised by intermediate heat flow (~50-65 mW/m^2); and c) old cratonic lithospheres with low surface heat flow (<~50 mW/m^2). The solidus of the shallow upper mantle is usually the pargasite dehydration solidus shallower than 3 GPa and the water saturated solidus deeper than 3 GPa. Geotherms are after Artemieva (2009) and Pollack and Chapman (1977). The intersection of the geotherm with these solidi indicates the appearance of partial melt. In the first two cases (a and b), the intersections mark the LAB, and for young cratons the mid-lithosphere discontinuity (MLD) where these boundaries are associated with the presence of partial melts at higher temperature and pressure. For old cratonic areas (c), however, the geotherm crosses the sub-solidus pargasite break-down curve indicating the MLD which separates fluid- and pargasite-rich upper mantle. Numbers in the hexagons indicate the following solidi: 1) Pargasite dehydration solidus (200 ppm < bulk 'water' < 0.4 wt.%); 2) Dry solidus (bulk 'water' < 200 ppm); 3) Water-saturated solidus (> 0.4 wt.%); 4) CO_2+H_2O bearing solidus; 5) Sub-solidus pargasite dehydration curve (modified after Fig. 10c in Green, 2015). Numbers in squares indicate sub-solidus reactions as follow: 1) olivine (Ol) + clinopyroxene (Cpx) + CO_2 → dolomite (Dol) + orthopyroxene (Opx); 2) Dol + orthopyroxene (Opx) → magnesite (Mag) + Cpx. Solid circles indicate the intersections of the geotherm and pargasite dehydration solidus. (d) Schematic representation of the relation between the LAB and MLD in various thermal-tectonic settings. The positions of pargasite-rich layers, ponded melts, and fluids and plumes are all highlighted. The figure is considerably modified after Fig. 1 in Rychert et al. (2020). The different tthermal-tectonic units are classified according to the three main scenarios above (a, b and c).

the LAB in young oceanic and continental lithospheres respectively. The base of the thermal lithosphere at 1300 °C is within the partial melt-bearing asthenosphere, where the viscosity may be even lower due to the higher degree of partial melting and lower effective viscosity of NAMs.

3) Under low surface heat flow conditions (<50 mW/m^2), the position of the LAB is below 100 km and is controlled by the intersection point of the geotherm and the water-saturated solidus. This thermal regime is characteristic for Early Proterozoic and older cratonic lithospheres. It is notable that all geotherms in this thermal regime intersect the sub-solidus pargasite dehydration curve (Fig. 2c). At this boundary pargasite breaks down to solid phases and 'water' rich fluids are liberated towards higher pressures. In contrast, the reaction takes place in the opposite direction as well when the pressure decreases. This boundary may account for the formation of MLDs at ~100 km in older cratonic lithospheres as discussed in the following section.

2.4. A brief overview of pertinent (geophysical) observations

2.4.1. LAB under younger oceanic and continental lithospheres

Green and Liebermann (1976) first proposed that the gradual thickening of the oceanic lithosphere is explained by the stability of pargasite up to ~1100°C at the pargasite dehydration solidus (Fig. 2). In their interpretation, the LAB beneath young oceanic plates is primarily a thermal boundary which coincides with the pargasite dehydration solidus. The thickening of oceanic plates is a consequence of thermal cooling and the associated subsidence of isotherms until a stable configuration is reached at ~90 km for oceanic plates older than 70 Ma.

Niu and Green (2018) investigated the depth of the oceanic seafloor (Crosby and McKenzie, 2009) and LAB (Kawakatsu et al., 2009) as a function of lithospheric age. They found that both depths become

basically constant after 70 Myrs. In addition, Niu and Green (2018) argued that the depth of the 1100 °C isotherm in half space cooling models matches well the seismologically characterised LAB with a 10% drop in shear wave velocities (Kawakatsu et al., 2009). It was also demonstrated that the major and trace element geochemistry of ocean island basalts (OIB) at the time of their eruption also follows a systematic trend with the LAB depth of the underlying oceanic plate. This variation in geochemistry reflects the changing width of the decompression interval (P_0−P_f), which is the interval between the depth where decompression melting begins (P_0) and the LAB where the upwelling terminates (P_f). Accordingly, OIB geochemistry in older and thicker oceanic plates shows lower melt fraction and higher pressure manifested in higher Ti, Mg Fe and lower Si and Al contents. Niu and Green (2018) implied that the constant thickness of oceanic lithospheres older than 70 Ma is due to small-scale convection below the LAB in the partially melted asthenosphere whose convective heat supply keeps thermal equilibrium with the conductive heat loss through the overlying solid oceanic lithosphere. The importance of small-scale convection in the upper mantle was discussed by Doin et al. (1997) and Ballmer et al. (2007) as well.

In a recent study, based on the analysis of a vast body of seismological data, Rychert et al. (2020) concluded that the LAB of oceanic lithospheres is around the depth of the 1100 °C isotherm which agrees well with the interpretation of other seismological studies (Rychert and Shearer, 2011; Schmerr, 2012). It was noted, however, that this temperature is much lower than what would follow from the classic thermal model, because melting begins at lower temperatures if the role of a 'trace' amount of water and hydrous phases is considered. Rychert et al. (2020) noted that for older oceanic plates and hot spot affected regions, the depth of this isotherm is more variable.

Kovács et al. (2017) found that the depth of the LAB, determined by seismological and magnetotelluric methodologies beneath the Pannonian Basin (Central Europe) coincides with the depth of the ~1100 °C isotherm based on surface heat flow and area specific geotherms (Lenkey et al., 2002). The Pannonian Basin has a recently (<20 Ma) extended continental lithosphere whose thickness can be even less than 50 km (e.g., Horváth, 1993; Posgay et al., 1995; Tari et al., 1999; Ádám and Wesztergom, 2001; Balázs et al., 2016)

2.4.2. Mid lithospheric discontinuities below old continental lithospheres

Beyond the implications for young oceanic and continental lithospheres, other potentially important plate tectonic consequences arise from the kink in the pargasite dehydration solidus and the stability of pargasite up to ~3 GPa (~100 km, Fig. 2c). This kink in the stability of the pargasitic amphibole might play an important role in the origin of major discontinuities within the lithospheric mantle such as the MLD at ~100 km depth beneath old continental lithospheres (i.e., cratons).

Thybo and Perchuk (1997) and Thybo (2006) showed the existence of a globally significant velocity anomaly, which is characterised by decreasing seismic velocities at ~100 km. Thybo (2006) argued that this anomaly can be explained by upper mantle temperatures approaching the solidus. This is an important discovery in solid Earth science as it indicates the existence of MLDs usually located at ~100 km depth especially under old continents. These discontinuities are characterised by slower propagation of seismic waves and higher electrical conductivities, focused in a narrow zone (up to a few kilometres), in the upper mantle between the Moho and the LAB (e.g., Rader et al., 2015; Selway et al., 2015; Saha and Dasgupta, 2019; Saha et al., 2021).

Intermediate-depth earthquakes usually occur in the upper mantle between ~70 and 300 km, and are commonly related to deformation and stress accumulation along Benioff-type subducted oceanic slabs (Astiz et al., 1988). However, in other continental collision settings, such as the Vrancea zone of the Carpathians in Romania (Eastern Europe) and the Hindu Kush (Central Asia), it is unlikely that intermediate-depth earthquakes are directly related to oceanic subduction (e.g., Cloetingh et al., 2004; Knapp et al., 2005; Mațenco, 2017; Molnar and Bendick, 2019). Geophysical anomalies occurring at mid-lithospheric discontinuities at ~100 km depth have been identified in several other locations worldwide including North America (Abt et al., 2010; Hansen et al., 2015), Africa (Selway et al., 2015) and China (Sun and Kennett, 2017).

A recent study on the frequent intermediate-depth earthquakes in the Hindu Kush revealed that the distribution of earthquake hypocentres changes at and below ~100 km depth along several cross sections (Molnar and Bendick, 2019). In addition, there is a smaller jump in strain rates at ~100 km depth in the upper mantle.

A similar pattern is observed along a ~NNW-SSE oriented section running from the Scythian to the Arabian plate through the Caucasus Mts. (Ismail-Zadeh et al., 2020), where a significant low velocity anomaly (up to 3%) extends down to the transition zone. At the flanks of this low velocity anomaly, high velocity lobes occur, which detachment appears to be close to ~100 km depth (Ismail-Zadeh et al., 2020).

Many studies have proposed that the delamination/decoupling of the lower part of the cratonic lithospheric mantle (i.e., the cratonic root) occurs at ~100 km depth (e.g., Wang et al., 2018; Wang and Kusky, 2019). Current models postulate that removal of cratonic roots commences at their edges and propagates inward along possible MLDs at ~100 km depth (Wang et al., 2018; Wang and Kusky, 2019). A similar delamination scenario may have affected the evolution of the Saharan Metacraton during its 'metacratonization' process (Abdelsalam et al., 2002; Liégeois et al., 2013). In addition, the upper part of the cratonic lithosphere can be dislocated from its root along MLDs due to far-field tectonic forces, such as the opening of oceanic basins (Wang et al., 2017). Therefore, many indications point to a narrow globally occurring intra-lithospheric horizon present at ~100 km depth in older continental lithospheres or in locked continental collision settings. This discontinuity may have an important role in facilitating delamination of the lower continental lithosphere and the genesis of intermediate-depth earthquakes. The geochemical explanation for worldwide observed or inferred MLDs is still a controversial topic. A hypothesis is presented in the next section for the origin of MLDs in these tectonic settings.

2.5. Introducing the 'pargasosphere' hypothesis

The roots of the 'pargasosphere' hypothesis go back to as far as the 70's with the papers of Green (1973) and Green and Liebermann (1976). The 'pargasosphere' hypothesis postulates that the rheological and geophysical contrast between the outermost rigid shell of the Earth and its deeper levels is primarily due to the stability of (pargasitic) amphibole even at trace amounts of bulk 'water' content (Green et al., 2010; Kovács et al., 2012). Pargasitic amphibole is stable at pressures and temperatures less than 3 GPa (corresponding to a depth of ~100 km) and ~1100 °C, respectively, if the bulk 'water' content remains between a few hundreds of ppm and ~0.4 wt. %, which is generally true for the ambient upper mantle (Fig. 2; Niida and Green, 1999; Green et al., 2010; 2015; Kovács et al., 2012, 2017). The first and foremost important feature of pargasite is that melts and fluids are usually present beyond its stability field in the upper mantle, but absent within it, as these phases are consumed by metasomatic reactions while crystallising pargasite. The pargasite-bearing and melt/fluid barren upper mantle, therefore, is rheologically stronger and can be referred to as the 'pargasosphere', a term proposed here for the first time (Fig. 2). Note that this term may appear to be somewhat arbitrary and subjective because other amphiboles with different compositions and wider stability fields also occur in the upper mantle. Likewise, phlogopite, carbonates and carbonatite melts are also important volatile bearing phases of the upper mantle. In the discussion section of this article it is explained why these phases may only play a subordinate and episodic role in influencing the melting relations, geophysical and rheological properties of the upper mantle and what justifies the introduction of the new term: 'pargasosphere'.

In young oceanic (<70 Ma) and continental (Late Proterozoic and younger) settings, the 'pargasosphere' overlaps perfectly with the seismically determined lithosphere. Nevertheless, it overlaps only partially

with the lithosphere in low heat flow areas (<50 mW/m^2) such as older orogenic areas and cratons where the lithosphere is thicker than ~100 km. Cratons are the oldest (>>500 Ma) and thickest (>150 km) type of continental lithospheres usually characterised by geochemically highly depleted and 'dry' lithospheric mantle (Griffin et al., 1999). The dry nature of the cratonic lithospheric mantle means that their NAMs contain very low (<<100 ppm) or even below the limit of detection (<~1 ppm) 'water' content apart from locally strongly metasomatised regions (e.g., Peslier et al., 2010, 2012; Doucet et al., 2014). This means that the bulk 'water' content remains typically below 200 ppm, implying that the solidus moves towards the dry solidus (Fig. 2). Consequently the geotherm remains below the solidus temperature and partial melting does not occur and the upper mantle remains sub-solidus. This is in agreement with the fact that the LAB is usually located much deeper than 100 km, and at a position where the geotherm intersects the water saturated solidus at deeper levels, where a sufficient amount of bulk 'water' is available. The geochemically depleted and dry nature of cratonic keels is related to their formation. According to the models, cratonic lithospheres were assembled mainly from the accumulation and amalgamation of Archean and Proterozoic mid-ocean ridges. To a lesser degree supra-subduction environments and plume emplacements may have been only subordinate (e.g., Pearson and Wittig, 2014; Perchuk et al., 2020). All of these tectonic settings in the Early Earth must have experienced a very high degree of melt extraction which left behind a geochemically strongly depleted and dry residue: the cratonic root. These characteristics make the cratonic root buoyant with respect to the asthenosphere and rheologically strong, ensuring the preservation of its lithospheric characteristics through time (e.g., Peslier et al., 2010; Xia et al., 2013, 2019). Note that upwelling fluids and melts cannot survive for a long period of time in these cratonic roots without being consumed during metasomatic reactions forming hydrous phases (e.g., Foley, 2008; Aulbach et al., 2017; Foley and Fischer, 2017).

In the stability field of pargasite, the bulk activity of 'water' in the upper mantle does not change significantly and remains low, similarly to higher pressures and temperatures where small amounts of incipient partial melts or fluids are present (Lamb and Popp, 2009; Kovács et al., 2012; Bonadiman et al., 2014; Demouchy and Bolfan-Casanova, 2016). The 'water' storage capacity of the solid upper mantle (NAMs + pargasite), however, dramatically increases from ~200 ppm to ~0.4 wt.% (i.e., 4000 ppm; e.g., Green et al., 2010). The activity of water, and therefore, the 'water' content of NAMs cannot increase significantly in the presence of pargasite as migrating hydrous melts and fluids in the upper mantle may form pargasitic amphibole during metasomatic interactions (e.g., O'Reilly and Griffin, 2013; Demouchy and Bolfan-Casanova, 2016). Pargasitic amphibole is, therefore, an effective solid state container of 'water' and incompatible elements in the upper mantle. Thus, it can metaphorically be considered as the 'pearl' of the upper mantle which grows around the invading melts/fluids upwelling from the underlying asthenosphere. This prevents and shields the rest of the ambient mantle from further rehydration and chemical alteration. The absence of melts increases the rheological strength of the upper mantle (e.g., Kohlstedt and Zimmerman, 1996; Tommasi et al., 2017). The 'water' content of NAMs in the 'pargasosphere', however, can decrease during melting (Hao et al., 2014, 2016; Aradi et al., 2017; Xia et al., 2019), decompression upwelling (Patkó et al., 2019) and interaction with CO_2-rich fluids and melts (Sokol et al., 2013). If depletion of 'water' in NAMs happens, it can also contribute to increasing strength due to the inverse 'hydrolitic weakening' effect at lower 'water' contents in NAMs (e.g., Dixon et al., 2004; Girard et al., 2013; Tielke et al., 2017). In contrast, in the asthenosphere, small amounts of incipient melt effectively keep the 'water' content of NAMs high and their mineral structure 'hydrolytically weakened' with respect to the overlying 'pargasosphere'. As argued by Faul (2001), the typical low fraction of incipient melts (<1 v/v%) remains immobile in the asthenosphere and can stay there even for a longer period of time. However, further research is required to resolve in detail the interconnectivity and mobility of melts in the upper mantle.

The 'pargasosphere' hypothesis leads to innovative and experimentally testable predictions regarding the origin of MLDs and associated weakness zones in older continental lithospheres at ~100 km depth. Namely, pargasitic amphibole ultimately breaks down at this depth if the temperature remains below 1100 °C (Fig. 2b and c). This happens at the sub-solidus pargasite dehydration curve which is virtually pressure-independent until it joins the water-saturated and pargasite dehydration solidi at ~1050 °C (Fig. 2c). This curve and the kink in the pargasite dehydration solidus at slightly lower pressures together play a very important role since subtle variations in either pressure or temperature (<15 °C) can cause a rapid (geologically instantaneous) fluid release or a higher degree of partial melting (~3 v/v%, Niida and Green, 1999). Thus, this boundary may constitute a very important and dynamically evolving horizon over geological times (Fig. 2d). For older cratons where the heat flow is low (<50 mW/m^2), sub-solidus pargasite breakdown triggered by even subtle changes in pressure leads to the liberation of a few tens of v/v% hydrous fluids based on mass balance. The presence of even this small amount of water-rich fluid can reduce the creep strength of the upper mantle by 1-2 orders of magnitude (Faul and Jackson, 2007). In addition, this small amount of hydrous fluid decreases the electrical resistivity by 1-2 orders of magnitude (Tarits, 1986) and shear wave velocity by 10–15% (Takei, 2002).

Another important feature is that (hydrous) melts or fluids rising from deeper levels of the upper mantle start crystallising pargasite once crossing this horizon at ~100 km. This means that the amount of pargasite (and subordinately pyroxenes and phlogopite) may increase considerably with time in the immediate vicinity of this horizon as it sequesters H_2O from upward-migrating melts and fluids (Fig. 3a-c). The maximum modal abundance of pargasite is limited by the bulk geochemistry of the upper mantle and cannot exceed ~30 v/v%, corresponding to ~0.6 wt. % (6000 ppm) 'water' at ~1–1.5 GPa and 1025 °C (Green, 2015). As both temperature and pressure increase, the modal abundance of pargasitic amphibole decreases but it can still reach ~10 v/v% at ~3 GPa and ~1100 °C (Niida and Green, 1999). Consequently, a narrow zone, likely spanning a few hundred meters to a few kilometres in thickness, can be enriched in pargasite along this horizon (Fig. 2a-c; Fig. 3). This process may be further enhanced by the possible porosity contrast between the fluid/melt-bearing deeper (higher porosity) and pargasite-bearing shallower (lower porosity) upper mantle, which may render melts and fluids to stall at this boundary (see also Katz and Weatherley, 2012; Kelemen and Hirth, 2012; Zhang et al., 2020). Sparks and Parmentier (1991) demonstrated that a high porosity, melt-bearing layer is formed beneath the solid mantle, where the thickness of the layer is determined by the buoyancy of the melt and the stress resisting decompression. A pargasite rich layer immediately at the bottom of the lithosphere can further inhibit the upwelling of melts and fluids from the asthenosphere.

The ~100 km discontinuity is characterised by a dynamic equilibrium between melting/break-down and crystallisation of pargasite. This is because even a small variation in pressure and/or temperature can lead to hydrous melting (increasing P-T), liberation of hydrous fluids (increasing pressure) and crystallisation of pargasite (decreasing temperature) (Fig. 2b-c; Fig. 3c-f). The small variation in pressure and temperature may be triggered by subtle deformations in the upper mantle related to several independent factors such as plate tectonic forces (compression and extension), as well as thermal and hydrous plumes (Beniest et al., 2017; François et al., 2018). During extension, the heat can be transferred faster, especially along a rift axis, which may trigger melting along this horizon at ~100 km (Fig. 3d). Compression induced by far field forces at edges of the lithosphere can cause its folding and therefore, certain parts of the lithosphere can be uplifted and other parts down-thrusted (Cloetingh and Burov, 2011). This results in an increase of temperature and pressure along synclines and decreasing temperature and pressure along anticlines, respectively, which can also trigger melting along the pre-existing pargasite-bearing MLD (Fig. 3e).

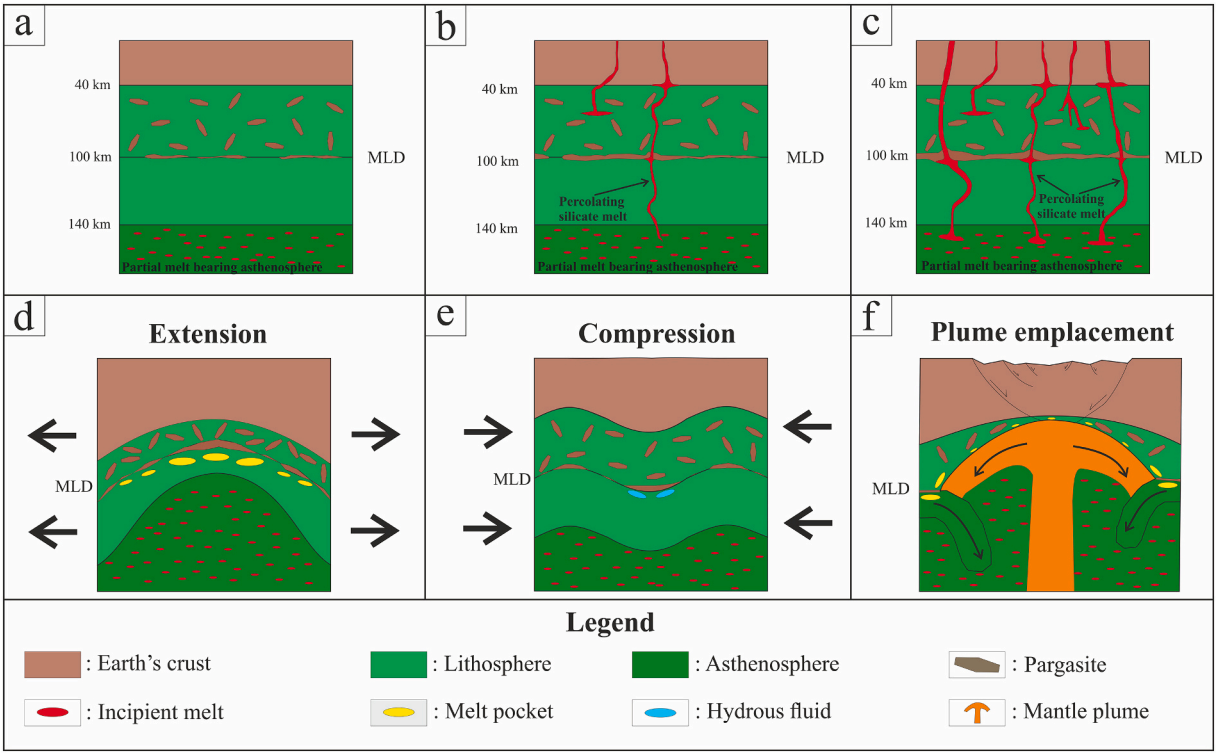

Fig. 3. Evolution of the MLD illustrated for old continental lithosphere (craton) in time (a-c) and during extension (d), compression (e) and mantle plume emplacement (f). a-c: Thickening of the pargasite-rich layer at 100 km with time in a cratonic area, as a result of silicate melts rising from the asthenosphere and crystallising pargasite during metasomatic reactions with the ambient mantle upon reaching the pargasite stability field. d-e: Melting or fluid release and decoupling related to the increased abundance of pargasite at the MLD induced by d) the thinning of the lithospheric mantle in an extensional regime; e) formation of anticlines and synclines in compressional regime during lithospheric scale folding; and f) slab delamination initiated by mantle plume emplacement along the MLD. (a-c) are modified after Kovács et al. (2017); (f) is modified after Burov and Cloetingh (2010).

Plumes (either thermal or hydrous) can also disturb the temperature and pressure conditions along the MLD and can initiate delamination of the lithosphere (Fig. 3f; Burov and Cloetingh, 2010). Recently, Cloetingh et al. (2021) proposed that the plume-induced delamination of the lower continental lithosphere may play an overlooked role in the initiation of subduction. Weakness zones at 100 km depth in old continental lithospheres can facilitate this delamination. Consequently, higher degrees of partial melting or fluid liberation along the MLD can be triggered by several tectonic forces, and the resulting melt or fluid layer could facilitate the decoupling of the pargasite-bearing upper part of the lithospheric mantle from the pargasite-free deeper one.

Another novelty of the pargasosphere hypothesis is that it may account for the LAB and MLD by combining the effect of a maximum few kilometres thick, pargasite-rich zone immediately underlain by hydrous melt- or fluid-bearing layers. Previous attempts (Selway et al., 2015; Rader et al., 2015; Rychert et al., 2020) usually aimed to model the origin of LAB and MLD by attributing a role only to one of these factors. The combined consideration of these factors is a novel element of our approach (see also the Discussion section).

3. Methods and parameters for the forward modelling of Vs and resistivity

To test how an increased amount of amphibole and accumulated melt or fluid around the boundary of pargasite stability would affect electrical resistivity and S-wave velocity in different tectonic settings, forward models for depth sections were constructed similarly to the approach of Selway et al. (2015). The forward models were constructed using geotherms for high (70 mW/m^2), intermediate (50 mW/m^2), and low (40 mW/m^2) heat flow regions respectively (Pollack and Chapman, 1977; Artemieva, 2009). Input parameters of the forward models and the resulting electrical resistivity and S-wave velocity profiles are presented in Supplementary Table 1.

Adopting modal proportions of the rock forming minerals, we assumed fertile (i.e., higher cpx/opx ratio) compositions for regions with high heat flow and more depleted for those with low heat flow. This is in accordance with compositional differences between sub-continental lithospheric mantle types with different ages for their last major crustal tectono-thermal event (Griffin et al., 2009). For low heat flow (cratonic) regions, we used modal compositions of the Kaapvaal Craton mantle (Griffin et al., 2009), taking into account the transition from spinel to garnet lherzolite at ~80 km (Downes, 1997). For the high heat flow (young oceanic or continental) regions, an average modal composition of xenoliths from the Carpathian-Pannonian region was used based on spinel lherzolite studies of Downes et al. (1992), Vaselli et al. (1995), Aradi et al. (2017) and Liptai et al. (2017). Modal compositions for intermediate heat flow regions were estimated as the average of the other two regions. Note that for simplicity, modal proportions were uniformly normalised to 100% at phase transitions. We assumed an exponentially increasing amphibole proportion (from 0.5 v/v% to 2, 5 or 10 v/v% depending on the different heat flow regions) towards the boundary of pargasite stability (~72 km at high heat flow regions, and ~100 km at intermediate and low heat flow regions; Fig. 2). Higher amounts of amphibole (up to 10 v/v%) are expected in older, cratonic regions than in young, oceanic or continental lithospheres (max. 2 v/v %). At higher pressures beyond the pargasite stability, a 1 v/v% melt is assumed for the high heat flow geotherm and 3 v/v% for the intermediate one, which then decreases to 1 v/v% within a ~2 km depth interval. In case of low heat flow regions, where the geotherm only intersects the subsolidus pargasite breakdown curve (Fig. 2), a small amount (~0.2 v/v%) of liberated aqueous fluid is assumed just below 100 km depth.

S-wave velocities were determined using the excel macro of Abers and Hacker (2016), and the effect of the melt was approximated using the experimental correlation determined by Chantel et al. (2016) (Supplementary Table 1). To calculate electrical resistivities, we used the excel worksheet modified after Kovács et al. (2018) (Supplementary Table 2), following the method and parametrisation of olivine, orthopyroxene, clinopyroxene and garnet by Fullea (2017). Experimentally derived parameters for amphibole were taken from Hu et al. (2018). The X_{Fe} ($X_{Fe} = 1 - Mg\#/100$) values of the silicates are based on geochemistry of spinel and garnet peridotites from the Siberian Craton

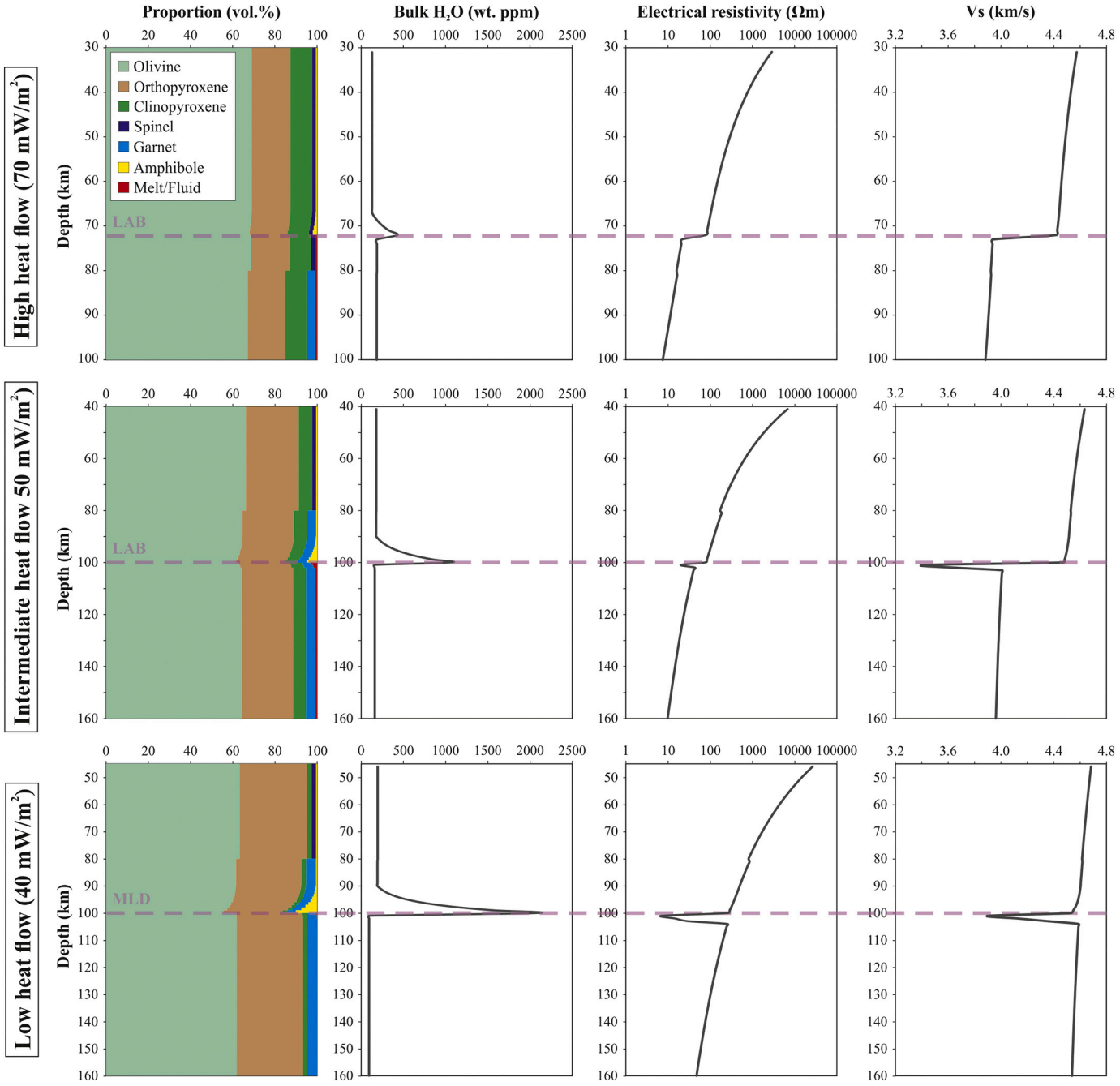

Fig. 4. Depth profiles of theoretical modal compositions, bulk 'water' contents, and forward models of electrical resistivity and shear wave velocity (V_s) in three lithosphere-asthenosphere columns characterised by different heat flows (Pollack and Chapman, 1977; Artemieva, 2009). Upper row: high heat flow (70 mW/m^2) representing young continental or oceanic environment, where the geotherm intersects the pargasite dehydration solidus at 1100°C (see Fig. 1) marking the LAB at ~70 km with the transition into incipient partial melting regime. Middle row: intermediate (50 mW/m^2) heat flow, representing old (Late Proterozoic – Early Paleozoic) continental plates, oceanic plates (>70 Ma) and young cratons. The LAB at ~100 km is defined by the pressure-controlled upper limit of pargasite stability (~3 GPa). Lower row: Early Proterozoic and older cratonic regions with low heat flow (40 mW/m^2), where the LAB is deeper than 100 km; the sub-solidus breakdown of pargasitic amphibole at ~100 km (3 GPa) marks the MLD with an increased (up to 10 v/v%) amphibole content directly underlain by a narrow layer with very small amount of (max. 0.2 v/v%) hydrous fluid. Electrical resistivities were calculated using the equation and parameterisation of Fullea (2017), integrating the effect of small melt fraction using the model of Sifré et al. (2014). S-wave velocity profiles were computed with the worksheet of Abers and Hacker (2016), and the effect of melt was estimated based on Chantel et al. (2016). The effect of fluid on electrical resistivity and S-wave velocity in case of the low heat flow regions was approximated using the studies of Tarits (1986) and Shiina et al. (2017), respectively. See text for further details and references on modal compositions and water contents of the three lithological columns.

(Ionov et al., 1993). For the water contents of NAMs within pargasite stability, we used the average values of off-craton and craton peridotites (Peslier, 2010) for intermediate and low heat flow regions, respectively. In regions with high heat flow, low water contents are assumed, such as in xenoliths from the central part of the Carpathian-Pannonian region (Liptai et al., 2021; Patkó et al., 2019). Since olivine water contents are often lost during or after transport to the surface, they were corrected using the general observation of $D_{cpx/ol}^{H_2O} = \sim 10$ (e.g., Demouchy and Bolfan-Casanova, 2016; Xia et al., 2019). To approximate water contents of NAMs below the depth of pargasite stability, we used the experimental data of Kovács et al. (2012).

The effect of a small fraction of melt on the electrical resistivity is calculated using the method of Sifré et al. (2014). In 1 v/v% melt, the H_2O content is about 2 wt.% considering 200 ppm water in the bulk peridotite, and the CO_2 content is 3000 ppm (Supplementary Table 1). For the intermediate heat flow regions, where a larger (3%) degree of melting is assumed immediately below the pargasite horizon, the H_2O and CO_2 of the melt is 3 wt.% and 1000 ppm, respectively. The large proportion of H_2O in the melt is attributed to the higher amount of pargasite (5 v/v%) in the bulk rock. The degree of partial melt is suggested to decrease in a narrow depth zone to 2–1 v/v% which is then considered constant for the asthenosphere, and H_2O and CO_2 contents change gradually to 2 wt.% and 3000 ppm, respectively (Supplementary Table 1). Note that the amount of CO_2 is constant as it does not partition in any solid phase. Therefore its proportion in the melt depends on the degree of partial melting. In regions with low heat flow, pargasite is expected to break down sub-solidus (Fig. 2), yielding a small fraction of aqueous fluid at 100 km (0.1 wt.% equalling to ~0.2 v/v%; Hack and Thompson, 2011). The effect of such a trace amount of aqueous fluid on electrical resistivity was approximated with the simplified equation (3) of Tarits (1986), assuming ~1 Ωm electrical resistivity of upper mantle fluids, which is extrapolated from lower pressure and temperature experimental results of Frantz and Marshall (1982). For the S-wave velocity (V_s) profile in the low heat flow regions, we adopted the empirical observations of Shiina et al. (2017), who suggested that a small amount of aqueous fluid can result in a 10-15 % decrease in seismic wave propagation speed. However, this is a very general and simplified approach, as the influence of mantle fluids on seismic velocities (and electrical resistivity as well) depends on other factors as well, such as salinity and aspect ratio of the pores (e.g., Marquis and Hyndman, 1992; Takei, 2002).

4. Results and discussion

4.1. Modelling results

Both electrical resistivity and shear wave velocity decrease with increasing depth as a result of increasing pressure and temperature (Fig. 4). The differences in the calculated values within the 'pargasosphere' are resulting from different modal compositions, i.e., the more fertile, high heat flow regions have the lowest resistivity and seismic velocity. Although amphibole was shown to have an important contribution in lowering S-wave velocities when present in ~25 v/v% in the model of Selway et al. (2015), such high proportions are not supported by experimental petrologic studies (Niida and Green, 1999). Our model, while following the same methodology as shown in Fig. 11a of Selway et al. (2015), is based on different starting compositions. We maximised the amphibole content at 10 v/v% in the low heat flow regions, where it could have enough time to accumulate as supported by experimental constraints. At this abundance, amphibole only has minimal influence on S-wave propagation (note the curve just above 100 km on the low heat flow profile, Fig. 4).

We assume the presence of melts/fluids immediately below the pargasite-bearing horizon, whereas Selway et al. (2015) considered a melt/fluid-free upper mantle. As our models show, a small fraction of melt/fluid has a significantly higher effect on both electrical resistivity and shear wave velocity than amphibole (Fig. 4). For regions with high heat flow, this appears as an instantaneous drop at the LAB from 80 to 22 Ωm and from 4.4 to 3.9 km/s, respectively. For intermediate heat flow regions, the assumed higher (3 v/v%) melt fraction, which is a consequence of higher amphibole proportion (see Section 3), results in a negative spike in resistivity and shear wave velocity before returning to the constant 1 v/v% melt content expected for the asthenosphere. This change, however, does not exceed one order of magnitude for electrical resistivity (from 78 to 20 Ωm). In cratonic regions, the increased amphibole content towards the MLD leads to the highest bulk water content. Thus below the subsolidus pargasite breakdown, the released aqueous fluid causes a sharp drop in both resistivity (from 263 to 7 Ωm) and S-wave velocity (from 4.5 to 3.8 km/s) in a narrow (1–2 km) depth range. For this latter case, above and below this horizon, the lithosphere can be considered 'dry'.

While we were aiming to be as realistic as possible in constructing these forward models, naturally, limitations and possible uncertainties still need to be taken into account. Modal compositions and water contents of NAMs may vary depending on the area of focus. In our models, we did not take into account compositional changes with depth and pressure dependence of water solubility in NAMs. Nevertheless, the above mentioned general observations and conclusions may still be valid. These results may also assist in the interpretation and refinement of geophysical inversions of seismic velocity and resistivity. A novel feature of our approach is that we take into account not only the enrichment of amphibole at the LAB and MLD, but emphasize the even more important role of silicate melts and fluids as well.

The results show that electrical resistivity has a significant drop of almost two orders of magnitude at 100 km depth and then it gradually returns to ambient values. The few deep magnetotellurics (MT) soundings, which are available from areas where the MLD was seismically confirmed in North America, show no obvious resistivity decrease at these depths (Selway, 2018). The resolving power of the MT methodology, especially at greater depths (>50 km), is limited and requires weeks-long undisturbed recordings. Thus, it is questionable whether a very thin well-conductive layer at ~100 km can be resolved using this methodology. Another possibility may be that melt-bearing lenses do not always form an interconnected and continuous network, but only transiently get connected during major tectonic events (such as earthquakes). All these limitations imply that deeper MT soundings or permanent MT stations are needed in areas where the MLD is seismically well-resolved to clarify whether conductivity variations are also associated with the MLD.

It is possible that fluids or melts (depending on the thermal regime) beneath the pargasite-rich MLD/LAB may not be distributed homogenously and their composition can also vary. In addition, these fluids and melts may not be always present but only if the tectonic forces and/or thermal perturbations create favourable physico-chemical conditions at the MLD/LAB level.

4.2. 'Controversies', uncertainties and open questions

4.2.1. The concentration of 'water' and the abundance of amphibole in the upper mantle

Amphiboles are thought to be stable in the upper mantle only if at least a few thousands ppm of bulk 'water' present (e.g., Grove et al., 2006; Saha et al., 2021). However, some experiments demonstrated that pargasite can be stable at bulk 'water' contents as low as a few hundreds of ppm (Asimow et al., 2004; Green et al., 2010; Kovács et al., 2012). This makes a significant difference in melting relations as the melting temperature of the pargasite-bearing upper mantle should be much lower (by 100–150 °C) than commonly assumed (Fig. 2). It is also argued in several studies that pargasite is not a common constituent of the upper mantle, and therefore unable to explain globally observed geophysical anomalies (Selway et al., 2015; Rader et al., 2015). Recent studies have addressed the concentration and constitution of 'water' in numerous

upper mantle xenoliths and their fluid inclusions, using micro-FTIR spectrometry (Aradi et al., 2017; Berkesi et al., 2019; Patkó et al., 2019). These studies using the very sensitive FTIR methodology concluded that pargasite is a more common constituent of the upper mantle than previously thought based on traditional optical microscopic observations only. Furthermore, pargasite can also occur as a tiny (a few microns or smaller) daughter phase in melt and fluid inclusions (Berkesi et al., 2019), lamellae in pyroxenes or along grain boundaries (Liptai et al., 2019). It remains yet to explain, however, why the presumably pargasite-enriched MLDs at 100 km are not sampled at all or only sporadically by mafic magmas coming from even deeper levels of the upper mantle. Nevertheless, the most important uncertainty that we still face is to determine accurately the lowest bulk water concentration at which pargasitic amphibole becomes stable in the upper mantle. We know from nominally 'dry' experiments with no added water that pargasite is stable to as low as ~200 ppm bulk water content. However, it is not yet known whether it is stabilised instantly when even a minute amount of 'water' is added, or only after the 'water' content in NAMs reaches a certain threshold. Resolving this question poses significant future challenges to experimentalists since achieving such very low bulk 'water' contents under laboratory conditions involves many technical obstacles.

4.2.2. The 'overlooked' carbon in the 'pargasosphere' hypothesis

Besides 'water', CO_2 is thought to be another fundamental volatile component in controlling the melting temperature and physical properties of the upper mantle (e.g., Dasgupta et al., 2013; Sifré et al., 2014; Dasgupta, 2018). The fact that carbon is virtually not soluble in silicate minerals (Shcheka et al., 2006) means that it has a limited but still appreciable effect on the solidus of the upper mantle shallower than ~70 km (decarbonation horizon), where carbon can be only present in fluids since solid carbonate minerals, carbonate and carbonated basaltic melts are not stable in these shallower regions of the upper mantle (Fig. 2; Green, 2015; Dasgupta, 2018). Very mobile carbonate and carbonated basaltic melts react at this horizon with the ambient upper mantle, producing CO_2-rich supercritical fluid, clinopyroxene and olivine and consuming orthopyroxene. Consequently, the modal composition of the upper mantle is shifted from lherzolitic towards wehrlitic composition. This decarbonation horizon is another prominent discontinuity in the shallower upper mantle (Fig. 2, Wallace and Green, 1988; Yaxley and Green, 1996; Yaxley et al., 1998). Aulbach et al. (2020) proposed that this wehrlitization process along the decarbonation horizon can be an important source of CO_2 emanations on the surface whose contribution to global geological CO_2 might not be negligible.

It may appear odd at first why the CO_2+H_2O solidus, which is usually ~100–150 °C below the water saturated solidus, has not been addressed in the 'pargasosphere' hypothesis. The answer lies in the very high mobility of carbonate or carbonated basaltic melts. Even if a very minute amount of such melt (~0.1 v/v%) is present in the upper mantle (which can be taken as a minimum estimate), then the carbonate and carbonated basaltic melts moves 3 and 1- 2 orders of magnitude faster respectively than hydrous basaltic melts and can still rise tens of kilometres during 1 Myr via porous flow (Gaillard et al., 2019). Consequently, carbonate and carbonated basaltic melts formed in the deeper upper mantle at the $CO_2 + H_2O$ solidus between 70 and 130 km (Fig. 2; Green, 2015) will raise to the decarbonation horizon almost instantaneously at geological time scales. Thus, even for thermal regimes under younger cratons carbon induces melting and is transported to the decarbonation horizon almost instantly. For this reason, it is more plausible that the solidus of the upper mantle is still the pargasite dehydration solidus below 70 km, as argued also by Green (2015). 'Water' is more compatible than carbon in the shallow upper mantle and has a longer residence time being incorporated as structural hydroxyl in NAMs or hydrous minerals. It is reasonable, nevertheless, that the transient presence of carbonate melts below 70 km can temporarily cause geophysical anomalies and weakening of mantle materials. In older cratons where the temperature is below the $CO_2 + H_2O$ solidus, carbon is present in solid carbonate minerals or as graphite or diamond depending on oxygen fugacity and pressure (Wallace and Green, 1988; Yaxley and Green, 1996; Yaxley et al., 1998; Foley and Fischer, 2017).

4.2.3. Other hydrous minerals

It is known that there are other hydrous minerals - such as phlogopite - in the upper mantle besides pargasitic amphibole, which could introduce some complexities to the phase assemblage and melting relations of the upper mantle. Phlogopite is stable up to higher pressures and temperatures than pargasitic amphibole (Kushiro et al., 1968; Konzett and Ulmer, 1999; Trønnes, 2002). The presence of phlogopite is widely considered to explain the origin of regional seismic discontinuities in the upper mantle (e.g., Rader et al., 2015; Selway et al., 2015; Saha and Dasgupta, 2019; Saha et al., 2021). However, the stabilisation of phlogopite requires significantly more potassium and 'water' than what is generally available in the ambient upper mantle. Phlogopite, pargasite and HZ lherzolite (i.e., ~average upper mantle composition defined by Hart and Zindler, 1986) usually contain ~10 wt.% potassium and 4 wt. % 'water', <1 wt.% potassium and 2 wt.% 'water', and 0.03 wt.% potassium and ~few hundreds ppm of 'water' respectively (Green et al., 2010). Cratonic peridotites contain maximum 0.3 wt.% bulk potassium (Saha et al., 2021) and a few hundreds of ppm 'water' in NAMs. This would mean only 3 wt.% phlogopite based on mass balance, but only if there was enough 'water', all potassium was incorporated in phlogopite and the K_2O/H_2O ratio was high. In most experiments, the stabilization and relatively high modal abundance (>5 v/v %) of phlogopite is achieved only by the addition of excess potassium (>0.5 wt.%) and 'water' (>1 wt.%). This means, however, that the bulk composition is no longer representative for the ambient upper mantle (Konzett and Ulmer, 1999; Green et al., 2010; Saha et al., 2021). Saha et al. (2021) reported <1.5–2.1 wt.% phlogopite in the vicinity of the cratonic MLD. However, they assumed that all the potassium is incorporated in phlogopite and thousands of ppm bulk 'water' is present. Since other potassium-bearing phases, such as amphibole, are common and bulk 'water' content in the cratonic upper mantle is significantly less (with the exception of subduction zones and strongly metasomatised regions), we conclude that the actual abundance of phlogopite in the ambient upper mantle is probably almost negligible. Its modal abundance, however, can be elevated locally via interaction with hydrous potassium-rich fluids or melts. Therefore, phlogopite is present only in more restricted, geochemically enriched regions of the upper mantle. Consequently, even in a best case scenario, phlogopite may provide only a minor contribution to the formation of global upper mantle discontinuities such as the MLD. The same consideration applies to potassium rich amphiboles (e.g., K-richterite).

In contrast, the stabilisation of pargasitic amphibole in the ambient upper mantle does not require the addition of any excess chemical element and its modal proportion can grow as high as maximum ~30 v/v% at the expense of NAMs if a few thousands ppm 'water' is present (Niida and Green, 1999). This is the reason why we prefer the term 'pargasosphere' which refers to the most common and abundant hydrous mineral of the shallow upper mantle.

4.2.4. Oxygen fugacity

Oxygen fugacity is known to have an important effect on the melting relations of the upper mantle (e.g., Foley, 2008, 2011; Green, 2015) The variation of oxygen fugacity alone can trigger partial melting even if other physical and chemical parameters remain unchanged. This process is referred to as the 'redox melting'. This melting mechanism occurs when rock bodies with different oxygen fugacities (i.e., remnants of highly oxidized subducted slabs and reduced ambient mantle) are in contact with each other and can yield hydrous silicate melts (Green, 2015). The redox conditions influence the composition of carbon bearing fluids, which in turn have a significant effect on the melting

relations of the upper mantle. The oxygen fugacity here is presented relative to the fayalite-magnetite-quartz buffer (FMQ, Ballhaus et al., 1990). According to Foley (2011), fluids are dominated by CH_4+H_2O (<FMQ (−4)), H_2O (FMQ (−4) <<FMQ (0)), and H_2O + CO_2 (>FMQ (0)) respectively in the order of increasing oxygen fugacity at ~ 3GPa and 1000 °C. The oxygen fugacity is usually FMQ (−1) – FMQ (0) in the 'pargasosphere' and FMQ (−1) – FMQ (−2) in cratonic keels at ~100 km. The asthenosphere is characterised by FMQ (−2) (Woodland and Koch, 2003; Foley, 2011; Green, 2015). Accordingly, the 'pargasophere' is dominated mainly by 'water'-bearing fluids with various dissolved CO_2 content which increases towards the surface (i.e., higher oxygen fugacity). This confirms the prime influence of 'water'-rich fluids on the solidus in the shallow upper mantle.

4.2.5. The role of different lithologies

Eclogite and pyroxenite are important additional lithologies in the predominantly peridotitic upper mantle (Le Roux et al., 2011; Lambart et al., 2016). Nevertheless, these lithologies constitute only a relatively small proportion of the convective asthenosphere with small spatial extent not expected to form coherent layers (up to maximum hundreds of metres; Bodinier et al., 2008). In contrast, they may form layers in the conductive lithosphere but are still unlikely to create globally uniform horizons as these layers are related to episodic and spatially and temporally incoherent melt percolations. The only exception may be the decarbonation horizon at ~70 km depth, where wehrlitization (i.e., a process increasing the modal proportion of clinopyroxene while decreasing that of orthopyroxene) may change the modal composition and lead to the accumulation of CO_2 rich fluids. This systematic shift in modal composition at this particular depth may lead to the generation of geophysically detectable discontinuities (Fig. 2d).

4.2.6. Compositional heterogeneities

The bulk major element composition of the peridotitic upper mantle influences the stability of pargasitic amphibole. The upper limit can vary between higher (~1150 °C) and lower (~1050 °C) temperatures in geochemically enriched and depleted upper mantle compositions respectively (Niida and Green, 1999). The maximum pressure until pargasite is stable is also known to change with bulk geochemistry (Mandler and Grove, 2016). This means that the exact position of the LAB and MLD both can vary (up to a few kilometres) according to the extent of geochemical heterogeneities in the upper mantle.

4.2.7. The role of latent heat

Both the melting at the pargasite dehydration solidus and the 'water'-rich fluid liberation at the sub-solidus pargasite break-down reaction are limited by latent heat (Stüwe, 1995). Latent heat is transferred usually by the thermal conduction of rocks above the LAB and MLD. Heat is thought to be transported by convection in the sublithospheric mantle. Thus, heat supply may be readily available at these boundaries in young oceans, continents and cratons (>50 mW/m^2) from the underlying molten and less viscous asthenosphere involved into the global convective movements. However, given that heat transfer in the lithosphere is mainly conductive, heat supply from the asthenosphere may be more limited in the old cratons. Alternatively, heat can be advected by melts and fluids derived from the sublithospheric mantle rocks. Considering however the typically low proportion of fluids and incipient partial melts in the upper mantle, these mobile phases may only play a subordinate role in heat transfer. Tectonic movements are known to sometimes generate heat by viscous heating (Burg and Gerya, 2005). However, there is still very little known about this process at the LAB and MLD in the upper mantle. Thus, it is an important future task to quantitatively constrain the heat balance of these phase transformations.

4.3. Origin of CO_2 emanations distant to active tectonism and volcanism

The pargasosphere concept may provide a new generic model for the formation of CO_2 emanations in intraplate settings distant from active volcanic areas. Active rifting is associated with coeval volcanism and gas emanations due to intensive decompression melting in the rising asthenosphere (Muirhead et al., 2020). Diffuse gas emanations with upper mantle origin may remain active in older/inactive rifted areas long after the cessation of active magmatism, even at some distance from former volcanic edifices (Kennedy and Van Soest, 2007; Fig. 5). The chemical and isotopic composition of CO_2-rich gas emanations in the vicinity of active and inactive continental volcanoes (related or not to active subduction) often show a direct upper mantle origin and only a moderate relationship to shallow crustal magma chamber processes or carbon reservoirs (Allard et al., 1997; Vaselli et al., 2002; Karlstrom et al., 2013; Boudoire et al., 2018; Kis et al., 2017, 2019). Diffuse gas emanations originating from the upper mantle also occur in inactive continental rifts and older oceanic areas where active volcanism ceased long ago (e.g., Frezzotti et al., 2009; Nickschick et al., 2015). Recent studies also found that CO_2 can escape along faults far away from active volcanoes, and long after volcanic activity ceased, but the quantitative contribution of such emanations to global CO_2 emission is very poorly constrained (Caracausi et al., 2015; Lee et al., 2016).

The 'pargasosphere' hypothesis can be utilised to explain the origin of CO_2 in these areas. During gradual cooling of the partially molten asthenosphere beneath young oceans and continents, a small amount (<1 v/v %) of H_2O- and CO_2-bearing basaltic silicate melts or supercritical fluids are crystallised or reacts with the shallower upper mantle respectively (Berkesi et al., 2019). Most components in these melts and fluids can be incorporated in crystallising silicate minerals and accessory phases (e.g., apatite, sulphide minerals). 'Water' facilitates and controls the crystallisation of pargasite, but it can also be incorporated in NAMs as structural hydroxyl. In contrast, at these relatively shallow mantle levels, carbonate minerals are not stable and carbon is not soluble in silicate minerals. A small proportion of carbon may be incorporated in apatite (Riker et al., 2018), but this proportion is quantitatively negligible. Consequently, the carbon is mostly stored as CO_2 in fluid inclusions of silicate minerals or in free fluids at grain boundaries. Such processes have been observed and reported on small scales for fluid inclusions hosted in upper mantle xenoliths, but no tectonic and global significance has been elucidated (Berkesi et al., 2012, 2019; Frezzotti and Touret, 2014). These processes explain the gradual accumulation and release of 'deep' CO_2 at larger scales in inactive continental rifts and older oceanic areas. The source of CO_2 (and other volatiles) is the in-situ partial melt or incipient fluid present in the cooling asthenosphere. This process can be effective until the 1100 °C isotherm reaches the bottom of the 'pargasosphere' at 100 km depth, where the thickening of the oceanic lithosphere usually comes to an end (Fig. 5c-d). This region of the upper mantle under inactive continental rifts and young oceanic basins, where fractionation and concentration of CO_2 in fluid inclusion takes place, may be referred to as the 'carbon filter' zone (Fig. 5).

The CO_2-rich fluids trapped in fluid inclusions or along grain boundaries eventually migrate to the surface from the upper mantle and contribute to the global carbon cycle. Previous studies addressing the evolution of fluid inclusions during the deformation of their solid host minerals (see Vityk et al., 2000 for quartz analogy) have addressed only crustal and artificial materials. In case of CO_2-rich inclusions in upper mantle rocks, the effect of nano-fracturization has been investigated to better understand the extent of CO_2 loss via the transport and cooling of xenoliths from the mantle to the surface (Viti and Frezzotti, 2001; Yamamoto et al., 2011). The implication of these studies is that during intense deformation of the host minerals, fluid inclusions and fluids present at grain boundaries may get interconnected, decrepitated or opened up via diffusion or dislocation creep. This means that CO_2-rich fluids can also be liberated along cleavages and migrate quickly along these cleavages and grain boundaries towards the surface. The spatially

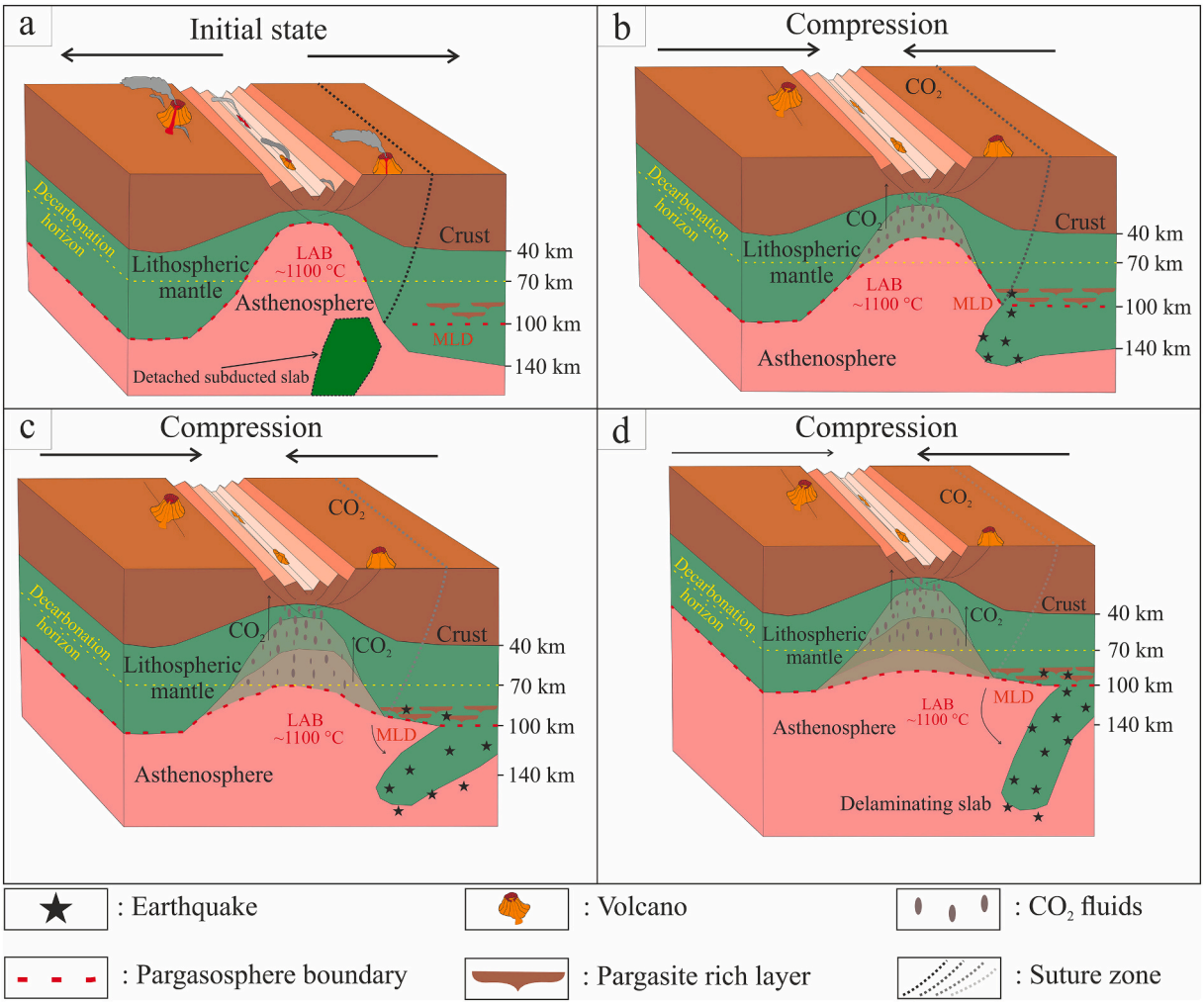

Fig. 5. Lithospheric mantle delamination along the MLD after the cessation of subduction (MLD) and lithospherisation of the asthenosphere in a compressional, post-extensional environment. The 1100 °C isotherm (red dashed line) represents the thermal boundary for pargasite. a) Initial state where volcanism is still active. Last remnants of a former subducted slab can still be detected. b) First stage of the post-volcanic phase in a compressional environment. The lower part of the lithospheric mantle starts to break off at the MLD, initiating earthquakes in the surrounding area. Lithospherisation of the asthenosphere results in CO_2 enrichment in the fluids that starts migrating towards the surface (see Fig. 2). c-d) Progression of delamination, lithospherisation and associated CO_2 degassing. The lithosphere-asthenosphere boundary subsides due to cooling of the asthenosphere, resulting in amphibole (pargasite) crystallisation. The section is not to scale. Brown lenses right above the MLD represent pargasite-rich zones (Rader et al., 2015; Kovács et al., 2017). The figure is modified after Berkesi et al. (2019).

and temporarily varying stress field in the vicinity of intermediate-depth earthquakes may have an impact on the migration of these CO_2-rich fluids (also as carriers of noble gases, such as helium and radon, and other dissolved components) by opening and closing effective migration paths. This is precisely the reason why CO_2 (and associated noble gas) monitoring is tentatively used in earthquake prediction research (Szakács, 2021). Combined with a number of geophysical, geochemical and other monitoring techniques, obtaining long-term time series on the modulation of mantle-originated surface-measured CO_2 fluxes offers promising perspectives for seismic prediction as reviewed recently (Szakács, 2021 and references therein). Therefore, it appears that the pargasosphere hypothesis can contribute to better understanding of the mantle origin of CO_2 in areas distant from active magmatism.

4.4. Applications to geodynamical modelling

As shown by numerical methods in thermo-mechanical geodynamic modelling (Gerya, 2010), partial melting and fluid liberation during dehydration might be key parameters controlling rock rheology, and therefore, system behaviour in both compressional (e.g., Gerya and Meilick, 2011) and extensional (e.g., Liao and Gerya, 2015) tectonic settings. Up to now, most of melting-equipped geodynamic models used either simplified parameterizations (e.g., Katz et al., 2003) or the anhydrous (dry) solidus presumption (e.g., Green, 2015). Incorporation of P-T conditions controlling partial melting according to the 'pargasosphere' hypothesis permits to develop a new generation of thermo-mechanical models that can reassess the role of partial melting in fundamental tectonic and geodynamic processes such as subduction (Gerya, 2011; van Hunen and Moyen, 2012; Stern and Gerya, 2018; Crameri et al., 2020), continental rifting and break-up (Gueydan et al., 2008; Brune, 2016; Brune et al., 2016; Tetreault and Buiter, 2018), and plume-lithosphere interactions (Ribe and Christensen, 1994; Burov and Cloetingh, 2009, 2010; Ballmer et al., 2013; Burov and Gerya, 2014; Koptev et al., 2015, 2018; Cloetingh et al., 2021).

Apart from a melting temperature which follows the pargasite dehydration solidus and the water-saturated solidus below and above the upper limit of pargasite stability at ~3 GPa (~100 km), respectively, the 'pargasosphere' hypothesis also intrinsically assumes an abrupt switch in the ductile rheology of the upper mantle from dry olivine to wet olivine flow law (Ranalli, 1995) at MLDs at ~100 km depth in intermediate thermal regimes (i.e., in all old oceanic and continental lithospheres with the exception of cratons). Thermo-mechanical

numerical models including a temperature-independent drop in the lithospheric mantle viscosity along MLDs might shed new light on the processes of rifting and destruction of cratons (Wenker and Beaumont, 2018), old and thick continental blocks which are distinctly different from Phanerozoic lithosphere (Griffin et al., 2009) by their high viscosity and neutral buoyancy (Jordan, 1975). Strong and buoyant cratons are seemingly protected against deformation and destruction (Lenardic et al., 2003; Yoshida, 2012). However, a loss of stability has been recognized for the North China Craton (Zhu et al., 2012; He, 2015) and North Atlantic Craton (Sand et al., 2009; Tappe et al., 2011) through detection of tectono-thermal events assosiated with intense modification of the lithosphere and widespread magmatism (e.g., Tang et al., 2013). New modelling approaches based on the 'pargasosphere' concept will probably play an important role in (re)addressing the question of the relative importance of MLDs in processes such as mantle delamination (Ueda et al., 2012; Li et al., 2016) and craton destruction (Zhu et al., 2017; Celli et al., 2020).

4.5. Application of the 'pargasosphere' hypothesis to the Vrancea seismogenic zone

A suitable area to test the pargasosphere hypothesis is the Eastern Carpathians and its associated Vrancea seismogenic zone of Europe (Fig. 6a). The Carpathian orogen evolved in a Mediterranean plate tectonic context that included the Middle Jurassic opening of a branch of the Alpine Tethys ocean and its subsequent closure starting in Cretaceous times (e.g., Schmid et al., 2020; van Hinsbergen et al., 2020). The onset of Cretaceous oceanic subduction started the accretion of sediments in a thin-skinned orogenic thrust-and-fault belt by emplacing, deforming and exhuming successively younger tectonic units until around 8–9 Ma (e.g., Matenco, 2017 and references therein). At the time when the back-arc extension recorded by the Pannonian Basin ceased, which started at around 20 Ma and was driven by the roll-back of the Carpathians slab and/or asthenospheric flow, the main crustal subduction zone was locked during the late stages of continental collision (e.g., Kovács et al., 2012; Horváth et al., 2015; Balázs et al., 2017). The most recent evolution has been driven by slab pull, steepening and delamination, which created differential vertical movements in the Carpathian

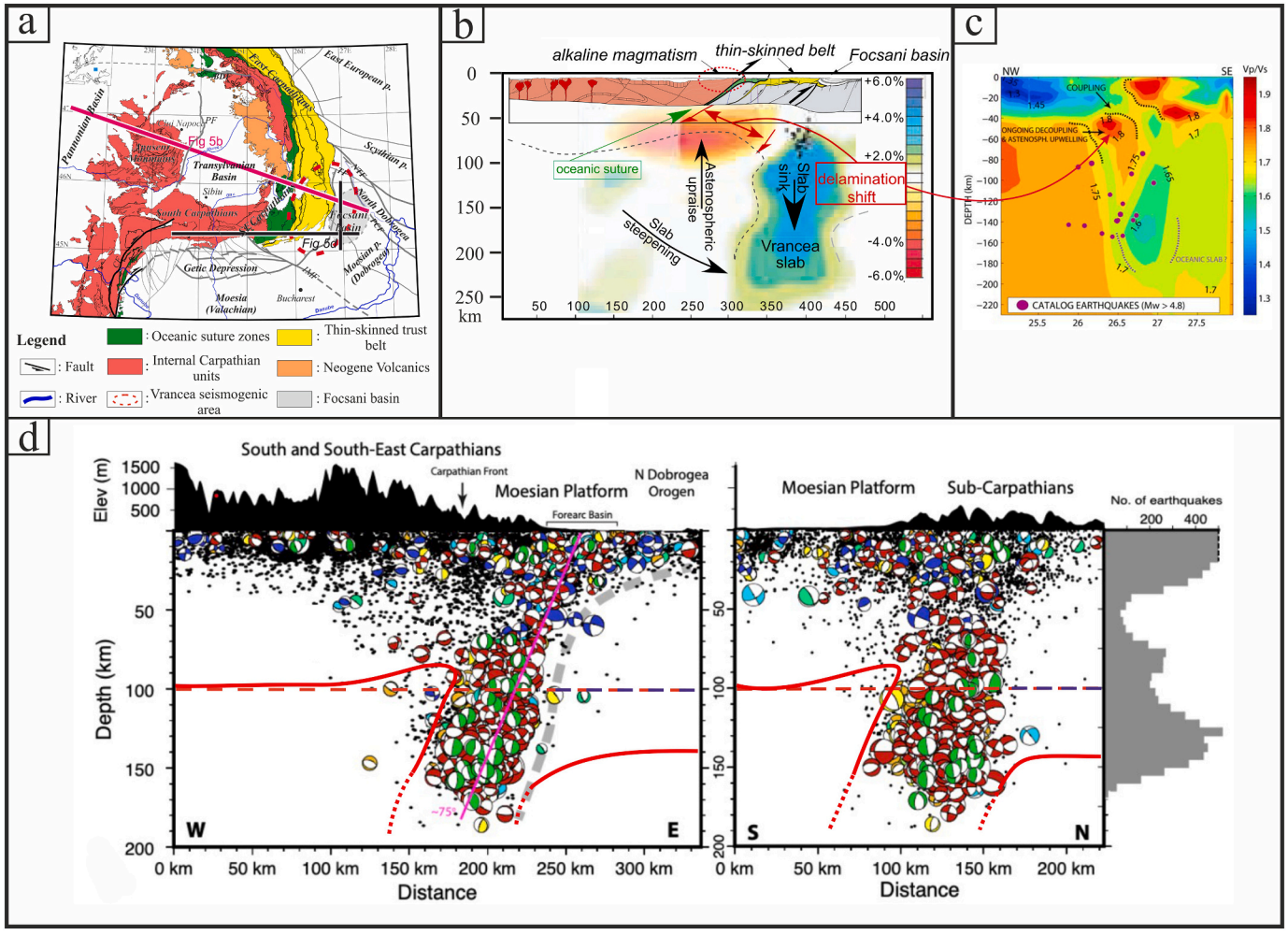

Fig. 6. a) Schematic map showing the geological context of the Vrancea zone and the main units discussed in the text. The figure is modified after Matenco (2017). IMF = Intra-Moesian Fault; TF = Trotus Fault; NTF = New Trotus Fault; PCF = Peceneaga-Camena Fault. Locations of cross sections in b) c) and d) are highlighted. b) NW-SE cross section along the SE Carpathians indicating the position of the asthenospheric upwelling (negative seismic velocity anomaly) and the delaminating Vrancea slab (positive seismic velocity anomaly) with the locations of intermediate-depth earthquakes. Suture zone in the crust and the position of the MLD are also indicated. The figure is modified after Tiliță et al. (2018). c) Vp/Vs model along the VRANCEA2001 refraction profile from Toni et al. (2009). Note the sudden decrease of this ratio in the seismogenic body at ~100 km depth. d) Distribution of different focal mechanisms for intermediate-depth earthquakes in the Vrancea seismogenic body along N-S and E-W cross sections. The potential position of the MLD at ~100 km is also highlighted. Not only the frequency of earthquakes, but also their physical properties change at the MLD. The figure is modified after Fig. 3b in Petrescu et al. (2021). LAB is marked by a solid red line, while the theoretical depth of the MLD is indicated by a dashed red line.

bend area characterized by foreland subsidence, leading to the presently observed 13 km deep Focsani foredeep, and uplift and exhumation in the orogenic wedge, associated with an asthenospheric upwelling in the immediate hinterland of the Vrancea slab (Fig. 6b; e.g., Tărăpoancă et al., 2003; Popa et al., 2005; Leever et al., 2006; Maţenco et al., 2007; Merten et al., 2010). The Vrancea area of the South-Eastern Carpathians is the present-day seismogenic expression of the Carpathians slab-detachment processes, confined in a 100 • 70 • 30 km^3 intermediate mantle volume and its overlying crust, releasing the highest strain in continental Europe, and is associated with a distinct positive anomaly in teleseismic mantle tomography studies (Fig. 6b; Wenzel et al., 1999; Radulian et al., 2000; Martin and Wenzel, 2006; Ismail-Zadeh et al., 2012). The continental nature of this slab inferred by geological studies is at the first sight at odds with geophysical interpretations, which suggest a subducted oceanic lithosphere (e.g., Knapp et al., 2005; Bokelmann and Rodler, 2014; Roban et al., 2020).

The pargasite and fluid or partial melt-bearing horizon at ~100 km depth may act as a prominent and localised weakness zone in the lithospheric mantle. The interaction of this layer with tectonic stresses modifies its pressure-temperature conditions and decouples the lithosphere, creating delamination of the part of the lithospheric mantle under slab buoyancy forces. This evolution provides a straightforward explanation of the conditions observed for the Carpathians slab and the present-day expression in the Vrancea seismic zone of the Carpathians (Fig. 6), where delamination has been inferred by a number of studies to explain the observed slab sinking geometry (see the review of Ismail-Zadeh et al., 2012). In contrast with most existing models, our hypothesis specifically states that pargasite-assisted delamination of the lower part of the lithospheric mantle could have been significantly active only after the 9–8 Ma times, when the crustal subduction plane was locked, although we cannot completely discard an earlier onset. The timing of (increased) delamination is justified by the onset of typical effects in terms of differential vertical movements associated with slab-pull and asthenospheric rise, and the gradual change in magmatism from calc-alkaline to adakitic-like and alkaline (Fig. 6, see also the discussion in Knapp et al., 2005; Seghedi et al., 2011; Ismail-Zadeh et al., 2012; Maţenco, 2017 and references therein). A pre-dating typical oceanic and continental subduction cannot be discarded due to the observation of MORB-type oceanic crust and overlying of deep-water sediments in the thin-skinned wedge (e.g., Schmid et al., 2020; Roban et al., 2020. It appears to be rather obvious that the post- 8–9 Ma evolution has ultimately created the presently observed ~50 km shift between the locations of the oceanic suture zone in the crust and the Vrancea slab in the upper mantle interpreted as the delaminating continental lower lithosphere.

We propose that the decoupling was initiated at, and has been taking place since 8–9 Ma along the MLD in the upper plate lithosphere, accreting its lower part to the subducting slab (see Fig. 5). The lower lithosphere accretion has increased the slab-pull and sinking effect, associated with the observed asthenospheric uprise in the hinterland delaminated zone. This scenario is supported by the observations that shallower and deeper seismogenic zones show distinct seismologic properties (Bazacliu and Radulian, 1999; Radulian et al., 2002), associated with a change in frequency - magnitude distribution and focal mechanisms of mantle earthquakes in the Vrancea zone at ~ 100 km depth (Fig. 6c-d; e.g., Bazacliu and Radulian, 1999; Radulian et al., 2002; Petrescu et al., 2021). A similar pattern was revealed by Tondi et al. (2009), who presented a 3D Vp/Vs model along the VRANCEA2001 refraction profile where they detected a decrease of this ratio at depths in excess of 100 km (Fig. 6c). Focal mechanisms and distribution of earthquakes appear to show a change at ~100 km, observed in shear wave velocity cross sections parallel and perpendicular to the SE Carpathians (Fig. 6d, Petrescu et al., 2021). According to their results, the Vp/Vs ratios show higher values (>1.75) NW of the Vrancea body mainly at depths shallower then 100 km, whereas the slab itself is characterised by lower values (<1.65) at depths below ~100 km (Fig. 6). Petrescu et al. (2021) found low stress ratios ($R = (\sigma_1-\sigma_2)/(\sigma_1-\sigma_3)$; Martnez-Garzón et al., 2014) for intermediate-depth Vrancea earthquakes which challenge the brittle failure mode of deformation. These authors argued that these observations can be better reconciled with the assumption of dehydration embrittlement which operates through increasing pore fluid pressure until failure occurs. The variability of seismic proxies observed around 100 km depth and the presence of fluids call directly for the application of the 'pargasosphere' concept in the explanation of these Vrancea earthquakes as being driven by a delamination process initiated by a former pargasite rich MLD at ~100 km depth. Fluids are inevitably liberated from both the 'subducted' lower continental lithospheric mantle and along the former MLD and migrate upward. The spatial and temporal pattern in the percolation of these fluids can contribute to the generation of intermediate-depth earthquakes. Thus, the 'pargasosphere' hypothesis may offer a novel geochemical and petrologic framework for new quantitative geodynamic models and geophysical interpretations.

5. Conclusions

The pargasosphere hypothesis implies that the lithosphere is usually mechanically stronger where pargasitic amphibole is stable. This is because nominally anhydrous minerals can contain less 'water' and melts are consumed in this region of the upper mantle by metasomatic reactions. Pargasitic amphibole is stable at pressures and temperatures less than 3 GPa and 1100 °C. Where the heat flow is high (>~70 mW/m^2), the pargasite stability (the pargasite dehydration solidus at ~1100 °C) marks the lithosphere-asthenosphere boundary (LAB) in young continental extensional and oceanic settings. According to the results of forward modelling, this is expected to result in a significant drop in both electrical resistivity and shear wave velocity at approximately ~70 km depth. In addition, the gradually cooling asthenosphere can be the source of CO_2 in young continental extensional and oceanic lithosphere due to the crystallisation of partial melts in the cooling asthenosphere. Pargasite contributes largely to the enrichment of CO_2 in the residual melt or fluid by sequestering 'water' out of the melt.

In areas with intermediate surface heat flow (~50–60 mW/m^2, older continental and oceanic plates), however, the stability of pargasitic amphibole at ~3 GPa and the kink in the pargasite dehydration solidus define the position of the LAB at ~100 km depth. Along this kink in the solidus, a minute change in pressure and/or temperature, caused by processes such as extension, compression, and plume emplacement, can trigger partial melting over a very small pressure and temperature interval. This results in a decrease of the electrical resistivity and a significant negative spike (−1.3 km/s) in shear wave velocity, which then returns to lower values due to the constant presence of a small degree of partial melt in the asthenosphere.

In cratonic regions, where the heat flow is low (~40 mW/m^2), the sub-solidus pargasite breakdown marks a horizon at ~ 100 km depth, where up to 10 v/v% pargasite can be accumulated, and underlain by liberated small fractions of hydrous fluids. Forward models show that this narrow zone with hydrous fluids accounts for negatives spikes both in electrical resistivity (as much as two magnitudes) and shear wave velocity. Therefore, it is likely that this horizon corresponds to the MLDs observed globally by geophysical studies at this depth. The MLDs sometimes identified at significantly different depths can be related to mechanisms other than amphibole accumulation. Nevertheless, this horizon at ~ 100 km can act as a privileged decoupling horizon, along which the lower part of the continental lithosphere can be delaminated (i.e., 'continental mantle subduction'; e.g., the seismic Vrancea zone, Romania), removed (destruction of cratonic roots, e.g., Eastern China) or shallow cratonic lithosphere can be displaced from its root (e.g., SW Africa). Due to its particular tectonic setting in a geodynamically active area of Eastern Europe, including seismicity and recent volcanism, the Vrancea seismic zone and its neighbourhood in the South-Eastern Carpathians (Romania) appears to be a promising target for testing and

applying the 'pargasosphere' hypothesis.

Supplementary data to this article can be found online at https://doi.org/10.1016/j.gloplacha.2021.103547.

Declaration of Competing Interest

The authors declare no competing interest.

Acknowledgements

We dedicate this article to the late Frank Horváth, who was a source of inspiration to all authors to integrate geological, geophysical and geochemical observations for better understanding of tectonic processes. We acknowledge the constructive and thoughtful comments of two anonymous reviewers. The time and attention of Zhengtang Guo for editorial handling is also acknowledged. We are greatly indebted to the TOPO-TRANSYLVANIA, TOPO-EUROPE and ILP community without whom this article could not have been realised. We thank the Editors of this special volume of GPC for inviting this article. The authors acknowledge the support of the MTA EK Lendület Pannon LitH$_2$Oscope grant, and the NKFIH NN128629 (TOPO-TRANSYLVANIA) grant. I.K. expresses his special thanks to David H. Green for sharing his vast body of knowledge on experimental petrology and melting relations of the upper mantle. Without the motivation by his pioneering ideas and discoveries this hypothesis could have been developed. Constructive discussions on geophysics and geodynamics with Antal Ádám, Szabolcs Harangi, László Fodor, Attila Balázs, Zoltán Erdős, Zsanett Pintér and Ylona van Dinther helped us to further develop our hypothesis. L. Patkó's and Cs. Szabó's work was funded by the Eötvös Loránd University (ELTE) Institutional Excellence Program (1783-3/2018/FEKUTSRAT) supported by the Hungarian Ministry of Human Capacities. S.A.P.L. Cloetingh was supported by the Distinguished Guest Scientist Fellowship Program of the Hungarian Academy of Sciences. T.P. Lange was supported by the GINOP-2.3.2-15-2016-00009 research program. This study is co-funded by an Alexander von Humboldt Foundation Fellowship to A. Koptev.

References

Abdelsalam, M.G., Liégeois, J.P., Stern, R.J., 2002. The saharan metacraton. J. Afr. Earth Sci. 34 (3-4), 119–136.

Abers, G.A., Hacker, B.R., 2016. A MATLAB toolbox and Excel workbook for calculating the densities, seismic wave speeds, and major element composition of minerals and rocks at pressure and temperature. Geochemistry, Geophysics, Geosystems 17, 616–624. https://doi.org/10.1002/2015GC006171.

Abt, D.L., Fischer, K.M., French, S.W., Ford, H.A., Yuan, H., Romanowicz, B., 2010. North American lithospheric discontinuity structure imaged by Ps and Sp receiver functions. J. Geophys. Res. Solid Earth 115, B09301. https://doi.org/10.1029/2009JB006914.

Ádám, A., Wesztergom, V., 2001. An attempt to map the depth of the electrical asthenosphere by deep magnetotelluric measurements in the Pannonian Basin (Hungary). Acta Geol. Hung. 44 (2-3), 167–192.

Aizawa, Y., Barnhoorn, A., Faul, U.H., Fitz Gerald, J.D., Jackson, I., Kovács, I., 2008. Seismic properties of Anita Bay dunite: an exploratory study of the influence of water. J. Petrol. 49 (4), 841–855.

Allard, P., Jean-Baptiste, P., D'Alessandro, W., Parello, F., Parisi, B., Flehoc, C., 1997. Mantle-derived helium and carbon in groundwaters and gases of Mount Etna, Italy. Earth Planet. Sci. Lett. 148 (3-4), 501–516. https://doi.org/10.1016/S0012-821X(97)00052-6.

Anderson, D.L., 1975. Accelerated plate tectonics. Science 187 (4181), 1077–1079.

Aradi, L.E., Hidas, K., Kovács, I.J., Tommasi, A., Klébesz, R., Garrido, C.J., Szabó, C., 2017. Fluid-enhanced annealing in the subcontinental lithospheric Mantle beneath the Westernmost margin of the Carpathian- Pannonian extensional basin system. Tectonics 36 (12), 2987–3011.

Artemieva, I.M., 2006. Global 1× 1 thermal model TC1 for the continental lithosphere: implications for lithosphere secular evolution. Tectonophysics 416 (1-4), 245–277.

Artemieva, I.M., 2009. The continental lithosphere: reconciling thermal, seismic, and petrologic data. Lithos 109 (1-2), 23–46.

Artemieva, I.M., Mooney, W.D., 2001. Thermal thickness and evolution of Precambrian lithosphere: a global study. J. Geophys. Res. Solid Earth 106 (B8), 16387–16414.

Artemieva, I.M., Billien, M., Lévêque, J.J., Mooney, W.D., 2004. Shear wave velocity, seismic attenuation, and thermal structure of the continental upper mantle. Geophys. J. Int. 157 (2), 607–628.

Asimow, P.D., Dixon, J.E., Langmuir, C.H., 2004. A hydrous melting and fractionation model for mid-ocean ridge basalts: application to the Mid-Atlantic Ridge near the Azores. Geochem. Geophys. Geosyst. 5 (1).

Astiz, L., Lay, T., Kanamori, H., 1988. Large intermediate-depth earthquakes and the subduction process. Phys. Earth Planet. Inter. 53, 80–166.

Aulbach, S., Massuyeau, M., Gaillard, F., 2017. Origins of cratonic mantle discontinuities: a view from petrology, geochemistry and thermodynamic models. Lithos 268, 364–382.

Aulbach, S., Lin, A.-B., Weiss, Y., Yaxley, G.M., 2020. Wehrlites from continental mantle monitor the passage and degassing of carbonated melts. Geochem. Perspect. Lett. 15, 30–34.

Austin, N.J., Evans, B., 2007. Paleowattmeters: a scaling relation for dynamically recrystallized grain size. Geology 35 (4), 343–346.

Balázs, A., Matenco, L., Magyar, I., Horváth, F., Cloetingh, S.A.P.L., 2016. The link between tectonics and sedimentation in back-arc basins: new genetic constraints from the analysis of the Pannonian Basin. Tectonics 35 (6), 1526–1559.

Balázs, A., Burov, E., Matenco, L., Vogt, K., François, T., Cloetingh, S., 2017. Symmetry during the syn- and post-rift evolution of extensional back-arc basins: the role of inherited orogenic structures. Earth Planet. Sci. Lett. 462, 86–98.

Ballhaus, C., Berry, R.F., Green, D.H., 1990. Oxygen fugacity controls in the Earth's upper mantle. Nature 348 (6300), 437–440.

Ballmer, M.D., Van Hunen, J., Ito, G., Tackley, P.J., Bianco, T.A., 2007. Non-hotspot volcano chains originating from small-scale sublithospheric convection. Geophys. Res. Lett. 34 (23).

Ballmer, M.D., Ito, G., Wolfe, C.J., Solomon, S.C., 2013. Double layering of a thermochemical plume in the upper mantle beneath Hawaii. Earth Planet. Sci. Lett. 376, 155–164.

Bazacliu, O., Radulian, M., 1999. Seismicity variations in depth and time in the Vrancea (Romania) subcrustal region. Nat. Hazards 19 (2-3), 165–177.

Behn, M.D., Hirth, G., Elsenbeck II, J.R., 2009. Implications of grain size evolution on the seismic structure of the oceanic upper mantle. Earth Planet. Sci. Lett. 282 (1-4), 178–189.

Beniest, A., Koptev, A., Leroy, S., Sassi, W., Guichet, X., 2017. Two-branch break-up systems by a single mantle plume: insights from numerical modeling. Geophys. Res. Lett. 44 (19), 9589–9597.

Beran, A., 1976. Messung des Ultrarot-Pleochroismus von Mineralen. XIV. Der Pleochroismus der OH-Streckfrequenz in Diopsid. Tschermaks Mineral. Petrogr. Mitt. 23 (2), 79–85.

Beran, A., Libowitzky, E., 2006. Water in natural mantle minerals II: olivine, garnet and accessory minerals. Rev. Mineral. Geochem. 62 (1), 169–191.

Berkesi, M., Guzmics, T., Szabó, C., Dubessy, J., Bodnar, R.J., Hidas, K., Ratter, K., 2012. The role of CO_2-rich fluids in trace element transport and metasomatism in the lithospheric mantle beneath the Central Pannonian Basin, Hungary, based on fluid inclusions in mantle xenoliths. Earth Planet. Sci. Lett. 331, 8–20.

Berkesi, M., Czuppon, G., Szabó, C., Kovács, I., Ferrero, S., Boiron, M.C., Peiffert, C., 2019. Pargasite in fluid inclusions of mantle xenoliths from northeast Australia (Mt. Quincan): evidence of interaction with asthenospheric fluid. Chem. Geol. 508, 182–196.

Blanchard, M., Ingrin, J., Balan, E., Kovács, I., Withers, A.C., 2017. Effect of iron and trivalent cations on OH defects in olivine. Am. Mineral. 102 (2), 302–311.

Bodinier, J.L., Garrido, C.J., Chanefo, I., Bruguier, O., Gervilla, F., 2008. Origin of pyroxenite–peridotite veined mantle by refertilization reactions: evidence from the Ronda peridotite (Southern Spain). J. Petrol. 49 (5), 999–1025.

Bokelmann, G., Rodler, F.-A., 2014. Nature of the Vrancea seismic zone (Eastern Carpathians) – New constraints from dispersion of first-arriving P-waves. Earth Planet. Sci. Lett. 390, 59–68.

Bonadiman, C., Nazzareni, S., Coltorti, M., Comodi, P., Giuli, G., Faccini, B., 2014. Crystal chemistry of amphiboles: implications for oxygen fugacity and water activity in lithospheric mantle beneath Victoria Land, Antarctica. Contrib. Mineral. Petrol. 167 (3), 984.

Boudoire, G., Rizzo, A.L., Di Muro, A., Grassa, F., Liuzzo, M., 2018. Extensive CO_2 degassing in the upper mantle beneath oceanic basaltic volcanoes: first insights from Piton de la Fournaise volcano (La Réunion Island). Geochim. Cosmochim. Acta 235, 376–401.

Brune, S., 2016. Rifts and rifted margins: a review of geodynamic processes and natural hazards. Plate Bound. Nat. Haz. 219, 13.

Brune, S., Williams, S.E., Butterworth, N.P., Müller, R.D., 2016. Abrupt plate accelerations shape rifted continental margins. Nature 536 (7615), 201–204.

Burg, J.P., Gerya, T.V., 2005. The role of viscous heating in Barrovian metamorphism of collisional orogens: thermomechanical models and application to the Lepontine Dome in the Central Alps. J. Metamorph. Geol. 23 (2), 75–95.

Burov, E., Cloetingh, S., 2009. Controls of mantle plumes and lithospheric folding on modes of intraplate continental tectonics: differences and similarities. Geophys. J. Int. 178 (3), 1691–1722.

Burov, E., Cloetingh, S., 2010. Plume-like upper mantle instabilities drive subduction initiation. Geophys. Res. Lett. 37 (3).

Burov, E., Gerya, T., 2014. Asymmetric three-dimensional topography over mantle plumes. Nature 513 (7516), 85–89.

Caracausi, A., Paternoster, M., Nuccio, P.M., 2015. Mantle CO_2 degassing at Mt. Vulture volcano (Italy): relationship between CO_2 outgassing of volcanoes and the time of their last eruption. Earth Planet. Sci. Lett. 411, 268–280.

Celli, N.L., Lebedev, S., Schaeffer, A.J., Gaina, C., 2020. African cratonic lithosphere carved by mantle plumes. Nat. Commun. 11 (1), 1–10.

Chantel, J., Manthilake, G., Andrault, D., Novella, D., Yu, T., Wang, Y., 2016. Experimental evidence supports mantle partial melting in the asthenosphere. Sci. Adv. 2 (5), e1600246.

Cline Ii, C.J., Faul, U.H., David, E.C., Berry, A.J., Jackson, I., 2018. Redox-influenced seismic properties of upper-mantle olivine. Nature 555 (7696), 355–358.
Cloetingh, S., Burov, E., 2011. Lithospheric folding and sedimentary basin evolution: a review and analysis of formation mechanisms. Basin Res. 23 (3), 257–290.
Cloetingh, S.A.P.L., Burov, E., Matenco, L., Toussaint, G., Bertotti, G., Andriessen, P.A.M., Wortel, M.J.R., Spakman, W., 2004. Thermo-mechanical controls on the mode of continental collision in the SE Carpathians (Romania). Earth Planet. Sci. Lett. 218, 57–76.
Cloetingh, S.A.P.L., Koptev, A., Kovács, I., Gerya, T., Beniest, A., Willingshofer, E., Ehlers, T.A., Andrić-Tomašević, N., Botsyun, S., Eizenhöfer, P.R., François, T., Beekman, F., 2021. Plume-induced sinking of intra-continental lithospheric mantle: an overlooked mechanism of subduction initiation? Geochem. Geophys. Geosyst. 22 (2), e2020GC009482.
Crameri, F., Magni, V., Domeier, M., Shephard, G.E., Chotalia, K., Cooper, G., Eakin, C. M., Greta Grima, A., Gürer, D., Király, Á., Mulyukova, E., Peters, K., Robert, B., Thielmann, M., 2020. A transdisciplinary and community-driven database to unravel subduction zone initiation. Nat. Commun. 11 (1), 1–14.
Crosby, A.G., McKenzie, D., 2009. An analysis of young ocean depth, gravity and global residual topography. Geophys. J. Int. 178 (3), 1198–1219.
Dasgupta, R., 2018. Volatile-bearing partial melts beneath oceans and continents–Where, how much, and of what compositions? Am. J. Sci. 318 (1), 141–165.
Dasgupta, R., Mallik, A., Tsuno, K., Withers, A.C., Hirth, G., Hirschmann, M.M., 2013. Carbon-dioxide-rich silicate melt in the Earth's upper mantle. Nature 493 (7431), 211–215. https://doi.org/10.1038/nature11731.
Davies, G.F., 1992. On the emergence of plate tectonics. Geology 20 (11), 963–966.
Davies, J.H., 2013. Global map of solid Earth surface heat flow. Geochem. Geophys. Geosyst. 14 (10), 4608–4622.
Davies, J.H., Davies, D.R., 2010. Earth's surface heat flux. Solid Earth 1 (1), 5–24.
Debayle, E., Bodin, T., Durand, S., Ricard, Y., 2020. Seismic evidence for partial melt below tectonic plates. Nature 586 (7830), 555–559.
Demouchy, S., Bolfan-Casanova, N., 2016. Distribution and transport of hydrogen in the lithospheric mantle: a review. Lithos 240, 402–425.
Demouchy, S., Tommasi, A., Barou, F., Mainprice, D., Cordier, P., 2012. Deformation of olivine in torsion under hydrous conditions. Phys. Earth Planet. Inter. 202, 56–70.
Denis, C.M., Alard, O., Demouchy, S., 2015. Water content and hydrogen behaviour during metasomatism in the uppermost mantle beneath Ray Pic volcano (Massif Central, France). Lithos 236, 256–274.
Dietz, R.S., 1962. Ocean-basin evolution by sea-floor spreading. In: Continental Drift, Vol. 3. Academic Press, New York, pp. 289–298.
Dixon, J.E., Leist, L., Langmuir, C., Schilling, J.G., 2002. Recycled dehydrated lithosphere observed in plume-influenced mid-ocean-ridge basalt. Nature 420 (6914), 385–389.
Dixon, J.E., Dixon, T.H., Bell, D.R., Malservisi, R., 2004. Lateral variation in upper mantle viscosity: role of water. Earth Planet. Sci. Lett. 222 (2), 451–467.
Doin, M.P., Fleitout, L., Christensen, U., 1997. Mantle convection and stabi-lity of depleted and undepleted continental lithosphere. J. Geophys. Res. 102, 2771–2787.
Doucet, L.S., Peslier, A.H., Ionov, D.A., Brandon, A.D., Golovin, A.V., Goncharov, A.G., Ashchepkov, I.V., 2014. High water contents in the Siberian cratonic mantle linked to metasomatism: An FTIR study of Udachnaya peridotite xenoliths. Geochim. Cosmochim. Acta 137, 159–187.
Downes, H., 1997. Shallow continental lithospheric mantle heterogeneity - petrological constraints. In: Fuchs, K. (Ed.), Upper Mantle Heterogeneities from Active and Passive Seismology. Springer, pp. 295–308.
Downes, H., Embey-Isztin, A., Thirlwall, M.F., 1992. Petrology and geochemistry of spinel peridotite xenoliths from the western Pannonian Basin (Hungary): evidence for an association between enrichment and texture in the upper mantle. Contrib. Mineral. Petrol. 109 (3), 340–354.
Duretz, T., Gerya, T.V., 2013. Slab detachment during continental collision: influence of crustal rheology and interaction with lithospheric delamination. Tectonophysics 602, 124–140.
Eaton, D.W., Darbyshire, F., Evans, R.L., Grütter, H., Jones, A.G., Yuan, X., 2009. The elusive lithosphere–asthenosphere boundary (LAB) beneath cratons. Lithos 109 (1-2), 1–22.
Faul, U.H., 2001. Melt retention and segregation beneath mid-ocean ridges. Nature 410 (6831), 920–923.
Faul, U.H., Jackson, I., 2007. Diffusion creep of dry, melt-free olivine. J. Geophys. Res. Solid Earth 112 (B4).
Fischer, K.M., Ford, H.A., Abt, D.L., Rychert, C.A., 2010. The lithosphere-asthenosphere boundary. Annu. Rev. Earth Planet. Sci. 38, 551–575.
Fjeldskaar, W., 1994. Viscosity and thickness of the asthenosphere detected from the Fennoscandian uplift. Earth Planet. Sci. Lett. 126 (4), 399–410.
Foley, S., 1991. High-pressure stability of the fluor-and hydroxy-endmembers of pargasite and K-richterite. Geochim. Cosmochim. Acta 55 (9), 2689–2694.
Foley, S.F., 2008. Rejuvenation and erosion of the cratonic lithosphere. Nat. Geosci. 1 (8), 503–510.
Foley, S.F., 2011. A reappraisal of redox melting in the Earth's mantle as a function of tectonic setting and time. J. Petrol. 52 (7-8), 1363–1391.
Foley, S.F., Fischer, T.P., 2017. An essential role for continental rifts and lithosphere in the deep carbon cycle. Nat. Geosci. 10 (12), 897–902.
François, T., Koptev, A., Cloetingh, S., Burov, E., Gerya, T., 2018. Plume-lithosphere interactions in rifted margin tectonic settings: inferences from thermo-mechanical modelling. Tectonophysics 746, 138–154.
Frantz, J.D., Marshall, W.L., 1982. Electrical conductances and ionization constants of calcium chloride and magnesium chloride in aqueous solutions at temperatures to 600°C and pressures to 4000 bar. Am. J. Sci. 282, 1666–1693.
Frezzotti, M.L., Touret, J.L., 2014. CO_2, carbonate-rich melts, and brines in the mantle. Geosci. Front. 5 (5), 697–710.
Frezzotti, M.L., Peccerillo, A., Panza, G., 2009. Carbonate metasomatism and CO2 lithosphere–asthenosphere degassing beneath the Western Mediterranean: an integrated model arising from petrological and geophysical data. Chem. Geol. 262 (1-2), 108–120.
Fullea, J., 2017. On joint modelling of electrical conductivity and other geophysical and petrological observables to infer the structure of the lithosphere and underlying upper mantle. Surv. Geophys. 38 (5), 963–1004.
Gaillard, F., Sator, N., Gardés, E., Guillot, B., Massuyeau, M., Sifré, D., Hammouda, T., Guillaume, R., 2019. In: Orcutt, Beth N., Daniel, Isabelle, Dasgupta, Rajdeep (Eds.), The Link between the Physical and Chemical Properties of Carbon-Bearing Melts and Their Application for Geophysical Imaging of Earth's Mantle. Deep Carbon: Past to Present. Cambridge University Press, pp. 163–187.
Garel, F., Thoraval, C., 2021. Lithosphere as a constant-velocity plate: chasing a dynamical LAB in a homogeneous mantle material. Phys. Earth Planet. Inter. 106710.
Gerya, T.V., 2010. Introduction to Numerical Geodynamic Modelling. Cambridge University, p. 484.
Gerya, T.V., Meilick, F.I., 2011. Geodynamic regimes of subduction under an active margin: effects of rheological weakening by fluids and melts. J. Metamorph. Geol. 29 (1), 7–31.
Gerya, T., 2011. Future directions in subduction modeling. J. Geodyn. 52 (5), 344–378.
Girard, J., Chen, J., Raterron, P., Holyoke, C.W., 2013. Hydrolytic weakening of olivine at mantle pressure: evidence of [100](010) slip system softening from single-crystal deformation experiments. Phys. Earth Planet. Inter. 216, 12–20.
Green, D.H., 1973. Conditions of melting of basanite magma from garnet peridotite. Earth Planet. Sci. Lett. 17 (2), 456–465.
Green, D.H., 2015. Experimental petrology of peridotites, including effects of water and carbon on melting in the Earth's upper mantle. Phys. Chem. Miner. 42 (2), 95–122.
Green, D.H., Liebermann, R.C., 1976. Phase equilibria and elastic properties of a pyrolite model for the oceanic upper mantle. Tectonophysics 32 (1-2), 61–92.
Green, D.H., Hibberson, W.O., Kovács, I., Rosenthal, A., 2010. Water and its influence on the lithosphere–asthenosphere boundary. Nature 467 (7314), 448–451.
Green, D.H., Hibberson, W.O., Rosenthal, A., Kovács, I., Yaxley, G.M., Falloon, T.J., Brink, F., 2014. Experimental study of the influence of water on melting and phase assemblages in the upper mantle. J. Petrol. 55 (10), 2067–2096.
Griffin, W.L., Doyle, B.J., Ryan, C.G., Pearson, N.J., O'Reilly, S.Y., Davies, R., Kivi, K., Van Achterbergh, E., Natapov, L.M., 1999. Layered mantle lithosphere in the Lac de Gras area, Slave craton: composition, structure and origin. J. Petrol. 40 (5), 705–727.
Griffin, W.L., O'reilly, S.Y., Afonso, J.C., Begg, G.C., 2009. The composition and evolution of lithospheric mantle: a re-evaluation and its tectonic implications. J. Petrol. 50 (7), 1185–1204.
Griggs, D., 1967. Hydrolytic weakening of quartz and other silicates. Geophys. J. Int. 14 (1-4), 19–31.
Grove, T.L., Chatterjee, N., Parman, S.W., Médard, E., 2006. The influence of H_2O on mantle wedge melting. Earth Planet. Sci. Lett. 249 (1-2), 74–89.
Gueydan, F., Morency, C., Brun, J.P., 2008. Continental rifting as a function of lithosphere mantle strength. Tectonophysics 460 (1-4), 83–93.
Hack, A.C., Thompson, A.B., 2011. Density and viscosity of hydrous magmas and related fluids and their role in subduction zone processes. J. Petrol. 52 (7-8), 1333–1362.
Hansen, S.M., Dueker, K., Schmandt, B., 2015. Thermal classification of lithospheric discontinuities beneath USArray. Earth Planet. Sci. Lett. 431, 36–47.
Hao, Y., Xia, Q., Li, Q., Chen, H., Feng, M., 2014. Partial melting control of water contents in the Cenozoic lithospheric mantle of the Cathaysia block of South China. Chem. Geol. 380, 7–19.
Hao, Y.T., Xia, Q.K., Tian, Z.Z., Liu, J., 2016. Mantle metasomatism did not modify the initial H2O content in peridotite xenoliths from the Tianchang basalts of eastern China. Lithos 260, 315–327.
Hart, S.R., Zindler, A., 1986. In search of a bulk-Earth composition. Chem. Geol. 57 (3-4), 247–267.
Hauri, E., Wang, J., Dixon, J.E., King, P.L., Mandeville, C., Newman, S., 2002. SIMS analysis of volatiles in silicate glasses: 1. Calibration, matrix effects and comparisons with FTIR. Chem. Geol. 183 (1-4), 99–114.
Hawthorne, F.C., Oberti, R., Harlow, G.E., Maresch, W.V., Martin, R.F., Schumacher, J. C., Welch, M.D., 2012. Nomenclature of the amphibole supergroup. Am. Mineral. 97 (11-12), 2031–2048.
He, L., 2015. Thermal regime of the North China Craton: implications for craton destruction. Earth Sci. Rev. 140, 14–26.
van Hinsbergen, D.J.J., Torsvik, T.H., Schmid, S.M., Matenco, L.C., Maffione, M., Vissers, R.L.M., Gürer, D., Spakman, W., 2020. Orogenic architecture of the Mediterranean region and kinematic reconstruction of its tectonic evolution since the Triassic. Gondwana Res. 81, 79–229.
Hirschmann, M.M., 2010. Partial melt in the oceanic low velocity zone. Phys. Earth Planet. Inter. 179 (1-2), 60–71.
Hopper, E., Fischer, K.M., 2015. The meaning of midlithospheric discontinuities: a case study in the northern US craton. Geochem. Geophys. Geosyst. 16 (12), 4057–4083.
Horváth, F., 1993. Towards a mechanical model for the formation of the Pannonian basin. Tectonophysics 226 (1-4), 333–357.
Horváth, F., Musitz, B., Balázs, A., Végh, A., Uhrin, A., Nádor, A., Koroknai, B., Pap, N., Tóth, T., Wórum, G., 2015. Evolution of the Pannonian basin and its geothermal resources. Geothermics 53, 328–352.
Hu, H., Dai, L., Li, H., Sun, W., Li, B., 2018. Effect of dehydrogenation on the electrical conductivity of Fe-bearing amphibole: implications for high conductivity anomalies in subduction zones and continental crust. Earth Planet. Sci. Lett. 498, 27–37.

van Hunen, J., Moyen, J.F., 2012. Archean subduction: fact or fiction? Annu. Rev. Earth Planet. Sci. 40, 195–219.
Ingrin, J., Skogby, H., 2000. Hydrogen in nominally anhydrous upper-mantle minerals: concentration levels and implications. Eur. J. Mineral. 12 (3), 543–570.
Ionov, D., Ashchepkov, I., Stosch, H.-G., Witt-Eickschen, G., Seck, H., 1993. Garnet peridotite xenoliths from the Vitim volcanic field, Baikal region: the nature of the garnet-spinel peridotite transition zone in the continental mantle. J. Petrol. 34, 1141–1175.
Ismail-Zadeh, A., Maţenco, L., Radulian, M., Cloetingh, S., Panza, G., 2012. Geodynamics and intermediate-depth seismicity in Vrancea (the south-eastern Carpathians): current state-of-the art. Tectonophysics 530-531, 50–79.
Ismail-Zadeh, A., Adamia, S., Chabukiani, A., Chelidze, T., Cloetingh, S., Floyd, M., Gorshkov, A., Gvishiani, A., Ismail-Zadeh, T., Kaban, M.K., Kadirov, F., Karapetyan, J., Kangarli, T., Kiria, J., Koulakov, I., Mosar, J., Mumladze, T., Müller, B., Sadradze, N., Safarov, R., Schilling, F., Soloviev, A., 2020. Geodynamics, seismicity, and seismic hazards of the Caucasus. Earth Sci. Rev. 207, 103222. https://doi.org/10.1016/j.earscirev.2020.103222.
Jones, A.G., Fullea, J., Evans, R.L., Muller, M.R., 2012. Water in cratonic lithosphere: calibrating laboratory-determined models of electrical conductivity of mantle minerals using geophysical and petrological observations. Geochem. Geophys. Geosyst. 13 (6).
Jordan, T.H., 1975. The continental tectosphere. Rev. Geophys. 13 (3), 1–12.
Karato, S.I., 2012. On the origin of the asthenosphere. Earth Planet. Sci. Lett. 321, 95–103.
Karato, S.I., 2014, May. Origin of the lithosphere-asthenosphere boundary (LAB) and the mid-lithosphere discontinuity (MLD). In: EGU General Assembly Conference Abstracts, p. 1355.
Karato, S.I., Olugboji, T., Park, J., 2015. Mechanisms and geologic significance of the mid-lithosphere discontinuity in the continents. Nat. Geosci. 8 (7), 509–514.
Karlstrom, K.E., Crossey, L.J., Hilton, D.R., Barry, P.H., 2013. Mantle ^{3}He and CO_2 degassing in carbonic and geothermal springs of Colorado and implications for neotectonics of the Rocky Mountains. Geology 41 (4), 495–498.
Kats, A., 1961. Hydrogen in Alpha Quartz. Dissertation. Delft University of Technology, Netherland.
Katz, R.F., Weatherley, S.M., 2012. Consequences of mantle heterogeneity for melt extraction at mid-ocean ridges. Earth Planet. Sci. Lett. 335, 226–237.
Katz, R.F., Spiegelman, M., Langmuir, C.H., 2003. A new parameterization of hydrous mantle melting. Geochem. Geophys. Geosyst. 4 (9), 1073. https://doi.org/10.1029/2002GC000433.
Kawakatsu, H., Kumar, P., Takei, Y., Shinohara, M., Kanazawa, T., Araki, E., Suyehiro, K., 2009. Seismic evidence for sharp lithosphere-asthenosphere boundaries of oceanic plates. Science 324 (5926), 499–502.
Kelemen, P.B., Hirth, G., 2012. Reaction-driven cracking during retrograde metamorphism: olivine hydration and carbonation. Earth Planet. Sci. Lett. 345, 81–89.
Kennedy, B.M., Van Soest, M.C., 2007. Flow of mantle fluids through the ductile lower crust: Helium isotope trends. Science 318 (5855), 1433–1436.
Kis, B.M., Ionescu, A., Cardellini, C., Harangi, S., Baciu, C., Caracausi, A., Viveiros, F., 2017. Quantification of carbon dioxide emissions of Ciomadul, the youngest volcano of the Carpathian-Pannonian Region (Eastern-Central Europe, Romania). J. Volcanol. Geotherm. Res. 341, 119–130.
Kis, B.M., Caracausi, A., Palcsu, L., Baciu, C., Ionescu, A., Futó, I., Sciarra, A., Harangi, S., 2019. Noble gas and carbon isotope systematics at the seemingly inactive Ciomadul volcano (Eastern-Central Europe, Romania): evidence for volcanic degassing. Geochem. Geophys. Geosyst. 20 (6), 3019–3043.
Knapp, J.H., Knapp, C.C., Raileanu, V., Maţenco, L., Mocanu, V., Dinu, C., 2005. Crustal constraints on the origin of mantle seismicity in the Vrancea Zone, Romania: The case for active continental lithospheric delamination. Tectonophysics 410 (1-4), 311–323.
Kohlstedt, D.L., 2006. The role of water in high-temperature rock deformation. Rev. Mineral. Geochem. 62 (1), 377–396.
Kohlstedt, D.L., Zimmerman, M.E., 1996. Rheology of partially molten mantle rocks. Annu. Rev. Earth Planet. Sci. 24 (1), 41–62.
Kohlstedt, D.L., Keppler, H., Rubie, D.C., 1996. Solubility of water in the α, β and γ phases of $(Mg,Fe)_2SiO_4$. Contrib. Mineral. Petrol. 123 (4), 345–357.
Konzett, J., 1997. Phase relations and chemistry of Ti-rich K-richterite-bearing mantle assemblages: an experimental study to 8.0 GPa in a Ti-KNCMASH system. Contrib. Mineral. Petrol. 128 (4), 385–404.
Konzett, J., Ulmer, P., 1999. The stability of hydrous potassic phases in lherzolitic mantle—an experimental study to 9.5 GPa in simplified and natural bulk compositions. J. Petrol. 40 (4), 629–652.
Koptev, A., Calais, E., Burov, E., Leroy, S., Gerya, T., 2015. Dual continental rift systems generated by plume–lithosphere interaction. Nat. Geosci. 8 (5), 388–392.
Koptev, A., Calais, E., Burov, E., Leroy, S., Gerya, T., 2018. Along-axis variations of rift width in a coupled lithosphere-mantle system, application to East Africa. Geophys. Res. Lett. 45 (11), 5362–5370.
Koptev, A.I., Ershov, A.V., 2010. The role of the gravitational potential of the lithosphere in the formation of a global stress field. Izvestiya Phys. Solid Earth 46 (12), 1080–1094.
Koptev, A.I., Ershov, A.V., 2011. Thermal thickness of the Earth's lithosphere: a numerical model. Mosc. Univ. Geol. Bull. 66 (5), 323–330.
Kovács, I., Hermann, J., O'Neill, H.S.C., Gerald, J.F., Sambridge, M., Horváth, G., 2008. Quantitative absorbance spectroscopy with unpolarized light: part II. Experimental evaluation and development of a protocol for quantitative analysis of mineral IR spectra. Am. Mineral. 93 (5-6), 765–778.
Kovács, I., O'Neill, H.S.C., Hermann, J., Hauri, E.H., 2010. Site-specific infrared OH absorption coefficients for water substitution into olivine. Am. Mineral. 95 (2-3), 292–299.
Kovács, I., Green, D.H., Rosenthal, A., Hermann, J., O'neill, H.S.C., Hibberson, W.O., Udvardi, B., 2012. An experimental study of water in nominally anhydrous minerals in the upper mantle near the water-saturated solidus. J. Petrol. 53 (10), 2067–2093.
Kovács, I., Lenkey, L., Green, D.H., Fancsik, T., Falus, G., Kiss, J., Orosz, L., Angyal, J., Vikor, Z., 2017. The role of pargasitic amphibole in the formation of major geophysical discontinuities in the shallow upper mantle. Acta Geodaetica Geophys. 52 (2), 183–204.
Kovács, I., Patkó, L., Falus, G., Aradi, L.E., Szanyi, G., Gráczer, Z., Szabó, C., 2018. Upper mantle xenoliths as sources of geophysical information: the Perşani Mts. area as a case study. Acta Geodaetica Geophys. 53 (3), 415–438.
Kovács, I., Patkó, L., Liptai, N., Lange, T.P., Taracsák, Z., Cloetingh, S.A.P.L., Török, K., Király, E., Karátson, D., Biró, T., Kiss, J., Zs, Pálos, Aradi, L., Gy, Falus, Hidas, K., Berkesi, M., Koptev, A., Novák, A., Wesztergom, V., Fancsik, T., Cs, Szabó, 2020. The role of water and compression in the genesis of alkaline basalts: inferences from the Carpathian-Pannonian region. Lithos 354, 105323.
Kushiro, I., Syono, Y., Akimoto, S.I., 1968. Melting of a peridotite nodule at high pressures and high water pressures. J. Geophys. Res. 73 (18), 6023–6029.
Lamb, W.M., Popp, R.K., 2009. Amphibole equilibria in mantle rocks: determining values of mantle a H2O and implications for mantle H_2O contents. Am. Mineral. 94 (1).
Lambart, S., Baker, M.B., Stolper, E.M., 2016. The role of pyroxenite in basalt genesis: melt-PX, a melting parameterization for mantle pyroxenites between 0.9 and 5 GPa. J. Geophys. Res. Solid Earth 121 (8), 5708–5735.
Le Roux, V., Dasgupta, R., Lee, C.T., 2011. Mineralogical heterogeneities in the Earth's mantle:constraints from Mn, Co, Ni and Zn partitioning during partial melting. Earth Planet. Sci. Lett. 307 (3-4), 395–408.41-52.
Leake, B.E., Woolley, A.R., Arps, C.E., Birch, W.D., Gilbert, M.C., Grice, J.D., Hawthorne, F.C., Kato, A., Kisch, H.J., Krivovichev, V.G., Linthout, K., 1997. Nomenclature of amphiboles; report of the subcommittee on amphiboles of the International Mineralogical association, commission on new minerals and mineral names. Can. Mineral. 35 (1), 219–246.
Lee, H., Muirhead, J., Fischer, T., Ebinger, C., Kattenhorn, S., Kianji, G., 2016. Tectonic degassing of mantle-derived CO_2 along faults in the East African Rift. Nat. Geosci. 9 (2), 145–149.
Leever, K.A., Matenco, L., Bertotti, G., Cloetingh, S., Drijkoningen, G.G., 2006. Late orogenic vertical movements in the Carpathian Bend Zone - seismic constraints on the transition zone from orogen to foredeep. Basin Res. 18 (4), 521–545.
Lenardic, A., Moresi, L.N., Mühlhaus, H., 2003. Longevity and stability of cratonic lithosphere: insights from numerical simulations of coupled mantle convection and continental tectonics. J. Geophys. Res. Solid Earth 108 (B6).
Lenkey, L., Dövényi, P., Horváth, F., Cloetingh, S.A.P.L., 2002. Geothermics of the Pannonian Basin and Its Bearing on the Neotectonics, 3. EGU Stephan Mueller Special Publication Series, pp. 29–40.
Li, Z.H., Liu, M., Gerya, T., 2016. Lithosphere delamination in continental collisional orogens: a systematic numerical study. J. Geophys. Res. Solid Earth 121 (7), 5186–5211.
Li, Z.X.A., Lee, C.T.A., Peslier, A.H., Lenardic, A., Mackwell, S.J., 2008. Water contents in mantle xenoliths from the Colorado Plateau and vicinity: implications for the mantle rheology and hydration-induced thinning of continental lithosphere. J. Geophys. Res. Solid Earth 113 (B9).
Liao, J., Gerya, T., 2015. From continental rifting to seafloor spreading: insight from 3D thermo-mechanical modeling. Gondwana Res. 28 (4), 1329–1343.
Libowitzky, E., Rossman, G.R., 1996. Principles of quantitative absorbance measurements in anisotropic crystals. Phys. Chem. Miner. 23 (6), 319–327.
Liégeois, J.P., Abdelsalam, M.G., Ennih, N., Ouabadi, A., 2013. Metacraton: nature, genesis and behavior. Gondwana Res. 23 (1), 220–237.
Liptai, N., Kovács, I.J., Lange, T.P., Pálos, Zs, Berkesi, M., Szabó, C., Wesztergom, V., 2019. Hyperspectral FTIR imaging as a method to detect volatile-bearing microphases in peridotite xenoliths from the Carpathian-Pannonian region. Goldschm. Abstr. 2019, 1981.
Liptai, N., Lange, T.P., Patkó, L., Pintér, Z., Berkesi, M., Aradi, L.E., Szabó, C., Kovács, I. J., 2021. Effect of water on the rheology of the lithospheric mantle in young extensional basin systems as shown by xenoliths from the Carpathian-Pannonian region. Glob. Planet. Chang. 196, 103364.
Liptai, N., Patkó, L., Kovács, I.J., Hidas, K., Pintér, Z., Jeffries, T., Zajacz, Z., O'Reilly, S. Y., Griffin, W.L., Pearson, N.J., Szabó, C., 2017. Multiple metasomatism beneath the Nógrád–Gömör Volcanic Field (Northern Pannonian Basin) revealed by upper mantle peridotite xenoliths. J. Petrol. 58 (6), 1107–1144.
Mackwell, S.J., Paterson, M.S., 1985. Water-related diffusion and deformation effects in quartz at pressures of 1500 and 300 MPa. Point Defects Min. 31, 141–150.
Mandler, B.E., Grove, T.L., 2016. Controls on the stability and composition of amphibole in the Earth's mantle. Contrib. Mineral. Petrol. 171 (8-9), 68.
Marquis, G., Hyndman, R.D., 1992. Geophysical support for aqueous fluids in the deep crust: seismic and electrical relationships. Geophys. J. Int. 110 (1), 91–105.
Martin, M., Wenzel, F., 2006. High-resolution teleseismic body wave tomography beneath SE-Romania - II. Imaging of a slab detachment scenario. Geophys. J. Int. 164 (3), 579–595.
Martnez-Garzón, P., Kwiatek, G., Ickrath, M., Bohnhoff, M., 2014. MSATSI: A MATLAB package for stress inversion combining solid classic methodology, a new simplified user-handling, and a visualization tool. Seismol. Res. Lett. 85 (4), 896–904.
Maţenco, L., 2017. Tectonics and Exhumation of Romanian Carpathians: Inferences from Kinematic and Thermochronological Studies. In: Radoane, M., Vespremeanu-Stroe, A. (Eds.), Landform Dynamics and Evolution in Romania. Springer International Publishing, pp. 15–56.

Maţenco, L., Bertotti, G., Leever, K., Cloetingh, S., Schmid, S., Tărăpoancă, M., Dinu, C., 2007. Large-scale deformation in a locked collisional boundary: Interplay between subsidence and uplift, intraplate stress, and inherited lithospheric structure in the late stage of the SE Carpathians evolution. Tectonics 26 (4), TC4011. https://doi.org/10.1029/2006TC001951.
McKenzie, D., 1978. Some remarks on the development of sedimentary basins. Earth Planet. Sci. Lett. 40 (1), 25–32.
McKenzie, D.P., 1967. Some remarks on heat flow and gravity anomalies. J. Geophys. Res. 72, 6261–6273.
Mei, S., Suzuki, A.M., Kohlstedt, D.L., Dixon, N.A., Durham, W.B., 2010. Experimental constraints on the strength of the lithospheric mantle. J. Geophys. Res. Solid Earth 115 (B8).
Merten, S., Maţenco, L., Foeken, J.P.T., Stuart, F.M., Andriessen, P.A.M., 2010. From nappe stacking to out-of-sequence postcollisional deformations: cretaceous to Quaternary exhumation history of the SE Carpathians assessed by low-temperature thermochronology. Tectonics 29 (3). https://doi.org/10.1029/2009tc002550.
Molnar, P., Bendick, R., 2019. Seismic moments of intermediate-depth earthquakes beneath the Hindu Kush: active stretching of a blob of sinking thickened mantle lithosphere? Tectonics 38 (5), 1651–1665.
Mosenfelder, J.L., Sharp, T.G., Asimow, P.D., Rossman, G.R., 2006. Hydrogen incorporation in natural mantle olivines. Am. Geophys. Union Geophys. Monograph Ser. 168, 45–56 doi:10.291168GM05.
Muirhead, J.D., Fischer, T.P., Oliva, S.J., Laizer, A., van Wijk, J., Currie, C.A., Lee, H., Judd, E.J., Kazimoto, E., Sano, Y., Takahata, N., 2020. Displaced cratonic mantle concentrates deep carbon during continental rifting. Nature 582 (7810), 67–72.
Nickschick, T., Kämpf, H., Flechsig, C., Mrlina, J., Heinicke, J., 2015. CO2 degassing in the Hartoušov mofette area, western Eger Rift, imaged by CO_2 mapping and geoelectrical and gravity surveys. Int. J. Earth Sci. 104 (8), 2107–2129.
Niida, K., Green, D.H., 1999. Stability and chemical composition of pargasitic amphibole in MORB pyrolite under upper mantle conditions. Contrib. Mineral. Petrol. 135 (1), 18–40.
Niu, Y., Green, D.H., 2018. The petrological control on the lithosphere-asthenosphere boundary (LAB) beneath ocean basins. Earth Sci. Rev. 185, 301–307.
O'Reilly, S.Y., Griffin, W.L., 2013. Mantle metasomatism. In: Harlov and Austrheim (Ed.), Metasomatism and the Chemical Transformation of Rock. Springer, Berlin, Heidelberg, pp. 471–533.
Patkó, L., Liptai, N., Kovács, I.J., Aradi, L., Xia, Q.-K., Ingrin, J., Mihály, J., O'Reilly, S., Griffin, W.L., Wesztergom, V., Szabó, C., 2019. Extremely low structural hydroxyl contents in upper mantle xenoliths from the Nógrád-Gömör Volcanic Field (northern Pannonian Basin): geodynamic implications and the role of post-eruptive re-equilibration. Chem. Geol. 507, 23–41.
Pearson, D.G., Wittig, N., 2014. The Formation and Evolution of Cratonic Mantle Lithosphere–Evidence from Mantle Xenoliths. https://doi.org/10.1016/B978-0-08-095975-7.00205-9.
Perchuk, A.L., Gerya, T.V., Zakharov, V.S., Griffin, W.L., 2020. Building cratonic keels in Precambrian plate tectonics. Nature 586 (7829), 395–401.
Peslier, A.H., 2010. A review of water contents of nominally anhydrous natural minerals in the mantles of Earth, Mars and the Moon. J. Volcanol. Geotherm. Res. 197 (1-4), 239–258.
Peslier, A.H., Woodland, A.B., Bell, D.R., Lazarov, M., 2010. Olivine water contents in the continental lithosphere and the longevity of cratons. Nature 467 (7311), 78–81.
Peslier, A.H., Woodland, A.B., Bell, D.R., Lazarov, M., Lapen, T.J., 2012. Metasomatic control of water contents in the Kaapvaal cratonic mantle. Geochim. Cosmochim. Acta 97, 213–246.
Peslier, A.H., Schönbächler, M., Busemann, H., Karato, S.I., 2017. Water in the Earth's interior: distribution and origin. Space Sci. Rev. 212 (1), 743–810.
Petrescu, L., Borleanu, F., Radulian, M., Ismail-Zadeh, A., Maţenco, L., 2021. Tectonic regimes and stress patterns in the Vrancea Seismic Zone: Insights into intermediate-depth earthquake nests in locked collisional settings. Tectonophysics 799, 228688.
Pollack, H.N., Chapman, D.S., 1977. On the regional variation of heat flow, geotherms, and lithospheric thickness. Tectonophysics 38 (3-4), 279–296.
Popa, M., Radulian, M., Grecu, B., Popescu, E., Placinta, A.O., 2005. Attenuation in Southeastern Carpathians area: result of upper mantle inhomogeneity. Tectonophyiscs 410, 235–249.
Posgay, K., Bodoky, T., Hegedüs, E., Kovácsvölgyi, S., Lenkey, L., Szafián, P., Takács, E., Tímár, Z.A., Varga, G., 1995. Asthenospheric structure beneath a Neogene basin in southeast Hungary. Tectonophysics 252 (1-4), 467–484.
Rader, E., Emry, E., Schmerr, N., Frost, D., Cheng, C., Menard, J., Yu, C.Q., Geist, D., 2015. Characterization and petrological constraints of the mid-lithospheric discontinuity. Geochem. Geophys. Geosyst. 16 (10), 3484–3504.
Radulian, M., Mandrescu, N., Panza, G.F., Popescu, E., Utale, A., 2000. Characterization of seismogenic zones of Romania. In: Panza, et al. (Eds.), Seismic hazards of the Circum-Pannonian region. Pure and Applied Geophysics, 2000. Birkhaeuser Verlag, Basel, Switzerland, pp. 55–77.
Radulian, M., Popescu, E., Bala, A., Utale, A., 2002. Catalog of fault plane solutions for the earthquakes occurred on the Romanian territory. Roman. J. Phys. 47 (5/6), 663–686.
Raff, A.D., Mason, R.G., 1961. Magnetic survey off the west coast of North America, 40 N. latitude to 52 N. latitude. Geol. Soc. Am. Bull. 72 (8), 1267–1270.
Ranalli, G., 1995. Rheology of the Earth. Chapman and Hall, London, p. 413.
Ribe, N.M., Christensen, U.R., 1994. Three-dimensional modeling of plume-lithosphere interaction. J. Geophys. Res. Solid Earth 99 (B1), 669–682.
Riker, J., Humphreys, M.C., Brooker, R.A., De Hoog, J.C., 2018. First measurements of OH-C exchange and temperature-dependent partitioning of OH and halogens in the system apatite–silicate melt. Am. Mineral. 103 (2), 260–270.
Roban, R.D., Ducea, M.N., Maţenco, L., Panaiotu, G.C., Profeta, L., Krézsek, C., Melinte-Dobrinescu, M.C., Anastasiu, N., Dimofte, D., Apotrosoaei, V., Francovschi, I., 2020. Lower cretaceous provenance and sedimentary deposition in the Eastern Carpathians: inferences for the evolution of the subducted oceanic domain and its European passive continental margin. Tectonics 39 (7) e2019TC005780.
Rossman, G.R., 2006. Analytical methods for measuring water in nominally anhydrous minerals. Rev. Mineral. Geochem. 62 (1), 1–28.
Royden, L., Keen, C.E., 1980. Rifting process and thermal evolution of the continental margin of eastern Canada determined from subsidence curves. Earth Planet. Sci. Lett. 51 (2), 343–361.
Rychert, C.A., Shearer, P.M., 2011. Imaging the lithosphere-asthenosphere boundary beneath the Pacific using SS waveform modeling. J. Geophys. Res. Solid Earth 116 (B7).
Rychert, C.A., Rondenay, S., Fischer, K.M., 2007. P-to-S and S-to-P imaging of a sharp lithosphere-asthenosphere boundary beneath eastern North America. J. Geophys. Res. Solid Earth 112 (B8).
Rychert, C.A., Schmerr, N., Harmon, N., 2012. The Pacific lithosphere-asthenosphere boundary: seismic imaging and anisotropic constraints from SS waveforms. Geochem. Geophys. Geosyst. 13 (9).
Rychert, C.A., Harmon, N., Constable, S., Wang, S., 2020. The nature of the lithosphere-asthenosphere boundary. J. Geophys. Res. Solid Earth 125 (10) p.e2018JB016463.
Saal, A.E., Hauri, E.H., Langmuir, C.H., Perfit, M.R., 2002. Vapour undersaturation in primitive mid-ocean-ridge basalt and the volatile content of Earth's upper mantle. Nature 419 (6906), 451–455.
Saha, S., Dasgupta, R., 2019. Phase relations of a depleted peridotite fluxed by a CO2-H2O fluid—implications for the stability of partial melts versus volatile-bearing mineral phases in the Cratonic Mantle. J. Geophys. Res. Solid Earth 124 (10), 10089–10106.
Saha, S., Peng, Y., Dasgupta, R., Mookherjee, M., Fischer, K.M., 2021. Assessing the presence of volatile-bearing mineral phases in the cratonic mantle as a possible cause of mid-lithospheric discontinuities. Earth Planet. Sci. Lett. 553, 116602.
Sand, K.K., Waight, T.E., Pearson, D.G., Nielsen, T.F., Makovicky, E., Hutchison, M.T., 2009. The lithospheric mantle below southern West Greenland: a geothermobarometric approach to diamond potential and mantle stratigraphy. Lithos 112, 1155–1166.
Schmerr, N., 2012. The Gutenberg discontinuity: melt at the lithosphere-asthenosphere boundary. Science 335 (6075), 1480–1483.
Schmid, S.M., et al., 2020. Tectonic units of the Alpine collision zone between Eastern Alps and western Turkey. Gondwana Res. 78, 308–374.
Seghedi, I., Maţenco, L., Downes, H., Mason, P.R.D., Szakács, A., Pécskay, Z., 2011. Tectonic significance of changes in post-subduction Pliocene-Quaternary magmatism in the south east part of the Carpathian-Pannonian Region. Tectonophysics 502 (1-2), 146–157.
Selway, K., 2018. Electrical discontinuities in the continental lithosphere imaged with magnetotellurics. In: Yuan, H., Romanowicz, B. (Eds.), Lithospheric Discontinuities. Wiley, pp. 89–109. https://doi.org/10.1002/9781119249740.ch5.
Selway, K., Ford, H., Kelemen, P., 2015. The seismic mid-lithosphere discontinuity. Earth Planet. Sci. Lett. 414, 45–57.
Shcheka, S.S., Wiedenbeck, M., Frost, D.J., Keppler, H., 2006. Carbon solubility in mantle minerals. Earth Planet. Sci. Lett. 245 (3-4), 730–742.
Shiina, T., Nakajima, J., Matsuzawa, T., Toyokuni, G., Kita, S., 2017. Depth variations in seismic velocity in the subducting crust: evidence for fluid-related embrittlement for intermediate-depth earthquakes. Geophys. Res. Lett. 44 (2), 810–817.
Sifré, D., Gardés, E., Massuyeau, M., Hashim, L., Hier-Majumder, S., Gaillard, F., 2014. Electrical conductivity during incipient melting in the oceanic low-velocity zone. Nature 509, 81–85.
Sokol, A.G., Kupriyanov, I.N., Palyanov, Y.N., 2013. Partitioning of H_2O between olivine and carbonate–silicate melts at 6.3 GPa and 1400 C: implications for kimberlite formation. Earth Planet. Sci. Lett. 383, 58–67.
Sparks, D.W., Parmentier, E.M., 1991. Melt extraction from the mantle beneath spreading centers. Earth Planet. Sci. Lett. 105 (4), 368–377.
Stalder, R., Ludwig, T., 2007. OH incorporation in synthetic diopside. Eur. J. Mineral. 19 (3), 373–380.
Stern, R.J., Gerya, T., 2018. Subduction initiation in nature and models: A review. Tectonophysics 746, 173–198.
Stüwe, K., 1995. Thermal buffering effects at the solidus. Implications for the equilibration of partially melted metamorphic rocks. Tectonophysics 248 (1-2), 39–51.
Sun, W., Kennett, B.L.N., 2017. Mid-lithosphere discontinuities beneath the western and central North China Craton. Geophys. Res. Lett. 44 (3), 1302–1310.
Szabó, C., Falus, G., Zajacz, Z., Kovács, I., Bali, E., 2004. Composition and evolution of lithosphere beneath the Carpathian–Pannonian Region: a review. Tectonophysics 393 (1-4), 119–137.
Szakács, A., 2021. Precursor-based earthquake prediction research: proposal for a Paradigm-shifting strategy. Front. Earth Sci. 8, 548398. https://doi.org/10.3389/feart.2020.548398.
Takei, Y., 2002. Effect of pore geometry on VP/VS: From equilibrium geometry to crack. J. Geophys. Res. Solid Earth 107 (B2). ECV-6.
Tang, Y.J., Zhang, H.F., Santosh, M., Ying, J.F., 2013. Differential destruction of the North China Craton: a tectonic perspective. J. Asian Earth Sci. 78, 71–82.
Tappe, S., Pearson, D.G., Nowell, G., Nielsen, T., Milstead, P., Muehlenbachs, K., 2011. A fresh isotopic look at Greenland kimberlites: cratonic mantle lithosphere imprint on deep source signal. Earth Planet. Sci. Lett. 305 (1–2), 235–248.
Tărăpoancă, M., Bertotti, G., Maţenco, L., Dinu, C., Cloetingh, S., 2003. Architecture of the Focsani depression: a 13 km deep basin in the Carpathians bend zone (Romania). Tectonics 22/6, 1074. https://doi.org/10.1029/2002TC001486.

Tari, G., Dövényi, P., Dunkl, I., Horváth, F., Lenkey, L., Stefanescu, M., Szafián, P., Tóth, T., 1999. Lithospheric structure of the Pannonian basin derived from seismic, gravity and geothermal data. Geol. Soc. Lond., Spec. Publ. 156 (1), 215–250.
Tarits, P., 1986. Conductivity and fluids in the oceanic upper mantle. Phys. Earth Planet. Inter. 42 (4), 215–226.
Tetreault, J.L., Buiter, S.J.H., 2018. The influence of extension rate and crustal rheology on the evolution of passive margins from rifting to break-up. Tectonophysics 746, 155–172.
Thybo, H., 2006. The heterogeneous upper mantle low velocity zone. Tectonophysics 416 (1-4), 53–79.
Thybo, H., Perchuk, E., 1997. The seismic 8 discontinuity and partial melting in continental mantle. Science 275 (5306), 1626–1629.
Tielke, J.A., Zimmerman, M.E., Kohlstedt, D.L., 2017. Hydrolytic weakening in olivine single crystals. J. Geophys. Res. Solid Earth 122 (5), 3465–3479.
Tommasi, A., Langone, A., Padrón-Navarta, J.A., Zanetti, A., Vauchez, A., 2017. Hydrous melts weaken the mantle, crystallization of pargasite and phlogopite does not: Insights from a petrostructural study of the Finero peridotites, southern Alps. Earth Planet. Sci. Lett. 477, 59–72.
Tondi, R., Achauer, U., Landes, M., Daví, R., Besutiu, L., 2009. Unveiling seismic and density structure beneath the Vrancea seismogenic zone, Romania. J. Geophys. Res. Solid Earth 114 (B11). https://doi.org/10.1029/2008JB005992.
Trønnes, R.G., 2002. Stability range and decomposition of potassic richterite and phlogopite end members at 5–15 GPa. Mineral. Petrol. 74 (2-4), 129–148.
Ueda, K., Gerya, T.V., Burg, J.P., 2012. Delamination in collisional orogens: thermomechanical modeling. J. Geophys. Res. Solid Earth 117 (B8).
Vaselli, O., Downes, H., Thirlwall, M., Dobosi, G., Coradossi, N., Seghedi, I., Szakacs, A., Vannucci, R., 1995. Ultramafic xenoliths in Plio-Pleistocene alkali basalts from the Eastern Transylvanian Basin: depleted mantle enriched by vein metasomatism. J. Petrol. 36 (1), 23–53.
Vaselli, O., Minissale, A., Tassi, F., Magro, G., Seghedi, I., Ioane, D., Szakacs, A., 2002. A geochemical traverse across the Eastern Carpathians (Romania): constraints on the origin and evolution of the mineral water and gas discharges. Chem. Geol. 182 (2-4), 637–654.
Viti, C., Frezzotti, M.L., 2001. Transmission electron microscopy applied to fluid inclusion investigations. Lithos 55 (1-4), 125–138.
Vityk, M.O., Bodnar, R.J., Doukhan, J.C., 2000. Synthetic fluid inclusions. XV. TEM investigation of plastic flow associated with reequilibration of fluid inclusions in natural quartz. Contrib. Mineral. Petrol. 139 (3), 285–297.
Wallace, M.E., Green, D.H., 1988. An experimental determination of primary carbonatite magma composition. Nature 335 (6188), 343–346.
Wang, Z., Kusky, T.M., 2019. The importance of a weak mid-lithospheric layer on the evolution of the cratonic lithosphere. Earth Sci. Rev. 190, 557–569.
Wang, Z., Kusky, T.M., Capitanio, F.A., 2017. Ancient continental lithosphere dislocated beneath ocean basins along the mid-lithosphere discontinuity: a hypothesis. Geophys. Res. Lett. 44 (18), 9253–9260.
Wang, Z., Kusky, T.M., Capitanio, F.A., 2018. On the role of lower crust and mid-lithosphere discontinuity for cratonic lithosphere delamination and recycling. Geophys. Res. Lett. 45 (15), 7425–7433.
Wenker, S., Beaumont, C., 2018. Can metasomatic weakening result in the rifting of cratons? Tectonophysics 746, 3–21.
Wenzel, F., Lorenz, F., Sperner, B., Oncescu, M.C., 1999. Seismotectonics of the Romanian Vrancea area. In: Wenzel, F., Lungu, D., Novak, O. (Eds.), Vrancea Earthquakes: Tectonics. Hazard and Risk Mitigation. Kluwer Academic Publishers, Dordrecht, Netherlands, pp. 15–26.
Woodland, A.B., Koch, M., 2003. Variation in oxygen fugacity with depth in the upper mantle beneath the Kaapvaal craton, Southern Africa. Earth Planet. Sci. Lett. 214 (1-2), 295–310.
Xia, Q.K., Liu, J., Liu, S.C., Kovács, I., Feng, M., Dang, L., 2013. High water content in Mesozoic primitive basalts of the North China Craton and implications on the destruction of cratonic mantle lithosphere. Earth Planet. Sci. Lett. 361, 85–97.
Xia, Q.K., Liu, J., Kovács, I., Hao, Y.T., Li, P., Yang, X.Z., Chen, H., Sheng, Y.M., 2019. Water in the upper mantle and deep crust of eastern China: concentration, distribution and implications. Natl. Sci. Rev. 6 (1), 125–144.
Yamamoto, J., Otsuka, K., Ohfuji, H., Ishibashi, H., Hirano, N., Kagi, H., 2011. Retentivity of CO2 in fluid inclusions in mantle minerals. Eur. J. Mineral. 23 (5), 805–815.
Yaxley, G.M., Green, D.H., 1996. Experimental reconstruction of sodic dolomitic carbonatite melts from metasomatised lithosphere. Contrib. Mineral. Petrol. 124 (3-4), 359–369.
Yaxley, G.M., Green, D.H., Kamenetsky, V., 1998. Carbonatite metasomatism in the southeastern Australian lithosphere. J. Petrol. 39 (11-12), 1917–1930.
Yoshida, M., 2012. Dynamic role of the rheological contrast between cratonic and oceanic lithospheres in the longevity of cratonic lithosphere: a three-dimensional numerical study. Tectonophysics 532, 156–166.
Zhang, N., Behn, M.D., Parmentier, E.M., Kincaid, C., 2020. Melt segregation and depletion during ascent of buoyant diapirs in subduction zones. J. Geophys. Res. Solid Earth 125 (2) p.e2019JB018203.
Zhu, R.X., Yang, J.H., Wu, F.Y., 2012. Timing of destruction of the North China Craton. Lithos 149, 51–60.
Zhu, R., Zhang, H., Zhu, G., Meng, Q., Fan, H., Yang, J., Zheng, T., 2017. Craton destruction and related resources. Int. J. Earth Sci. 106 (7), 2233–2257.